PHENOTYPIC MAPPING OF MEDULLARY THYMIC EPITHELIAL CELL PATTERNING IN PERINATAL AND ADULT INTACT THYMI

by

ERIN J. BAKER

(Under the Direction of Nancy Manley)

ABSTRACT

The thymus is a primary lymphoid organ that establishes and maintains the stromal microenvironments required for the development of self-tolerant, functional T cells. This microenvironment is comprised primarily of TECs and is essential for T cell development, differentiation, and proliferation. Identifying, functionally characterizing, and mapping TEC patterning throughout the developmental program is vital to understanding thymus organogenesis (development), homeostasis (maintenance), and involution (age related diminished activity). An alteration in immune response can arise from a variety of medical conditions ranging from inflammation to autoimmunity to immune deficiency to leukemia. Once a person has entered into early adulthood the thymus is already undergoing a reduction in thymus size and function termed age-associated involution, the functional impacts of this decline are not significant until late middle age in humans. Therefore, characterizing TEC pattern shifts in the involuting thymus and investigating how TEC motifs diverge from the homeostatic program is paramount to understanding not only the structure of the peripheral T cell pool and its

ability to generate an immune response, but also how it breaks down in disease or aging. Thymus heterogeneity has undoubtedly complicated investigations of the molecular and cellular events underlying the organ's development, homeostasis, and involution. Thus, there is a critical need for a comprehensive examination into the localization and covariance of the cellular components of the microenvironment on an organ-wide scale. This body of work was designed to fill this unmet need by investigating the three-dimensional architecture of the thymus and generating multidimensional maps of microscale interactions in the context of macroscale anatomical structures and networks offering insights in to the aging thymus and its corresponding diminished immune response.

INDEX WORDS: Thymus, organ development, Thymic epithelial cells (TEC), mTECs, thymic involution, homeostasis, tissue patterning, vasculature, innervation, cellular differentiation

PHENOTYPIC MAPPING AND FUNCTIONAL CHARACTERIZATION OF THYMIC EPITHELIAL CELL PATTERNING IN PERINATAL AND ADULT INTACT THYMI

By

ERIN J. BAKER

BA, St. Petersburg College, 2014

A Dissertation Submitted to the Graduate Faculty of The University of Georgia in Partial Fulfillment of the Requirements for the Degree

DOCTOR OF PHILOSOPHY

ATHENS, GEORGIA

2021

THYMIC EPITHELIAL CELL PATTERNING IN INTACT THYMI

by

ERIN J. BAKER

Major Professor:	Nancy Manley
Committee:	Jonathan Eggenschwiler
	Brian Condie
	Peter Kner
	Hongxiang Liu

Electronic Version Approved:

Ron Walcott
Vice Provost for Graduate Education and Dean of the Graduate School
The University of Georgia
May 2021

DEDICATION

I dedicate this dissertation to my family. Their unwavering support saw me through this challenging and rewarding process. I will be forever grateful and indebted to them. To my husband I know this process was trying at times. Thank you for always being my rock and support system. I will be forever grateful for your love. I also dedicate this to my major professor, Nancy Manley, whose passion for science, guidance, and belief in me as a researcher kept us on course even as a global pandemic threw everything into a tailspin.

ACKNOWLEDGEMENTS

This dissertation would not have been possible without the generous support of the NIH-T32 training grant in genetics, the ARCS scholarship, and the Genetics Department and Graduate school here at UGA. These entities set me on path to achieve all of goals and thank you will simply never be enough. I would also like to thank Manley/Condie Labs and the Lab of Ken Dorshkind. We have successfully maneuvered around countless obstacles by working as a team and supporting one another. I wish everyone continued success and I am grateful to call you all both friends and colleagues.

TABLE OF CONTENTS

Page

LIST OF FIGURES

Chapter 2

Page

Chapter 3

Page

Chapter 4

Page

CHAPTER 1

INTRODUCTION

The thymus serves as the biological site of T cell maturation and differentiation and a multitude of cellular and molecular interactions work in concert to oversee the thymus developmental program [1-4]. The propensity for tissues and organs to undertake a particular developmental pathway can be directed through various autonomous or conditional signaling pathways. Highly organized life stage switches can be triggered by the cell cycle or by a variety of developmental factors that influence cell type/fate. When the cellular and molecular environment is primed to interpret changing developmental cues, differentiation can occur and this in turn induces changes in cellular neighborhoods which can often lead to dynamic shifts in the patterning of a particular compartment. Previous research has demonstrated that during thymus organogenesis cell cycle dependent and cell cycle independent pathways drive growth and differentiation in a TEC-specific manner [5,6]. These data suggest that cell cycle machinery regulates FoxN1 gene expression levels to generate a dynamic range of expression, which in turn regulates the TEC developmental machinery to generate the diversity of TEC subsets, thus defining the transition from perinatal to adult thymus microenvironments and the establishment of homeostasis. Failure of homeostasis and the resulting degenerative process of aging-related involution is also driven by changes in the dynamic range of *Foxn1* expression, resulting in changes in TEC differentiation and compartment organization that reduce T

cell output and lead to immunosenescence. However, much about the organization and cellular diversity of the thymic microenvironment remains unclear, and thus the impacts of these molecular and functional changes across the lifespan on the function of the immune system remain to be discovered.

Thymus Function and It's Role in the Adaptive Immune System

The thymus is a highly specialized bilobed primary lymphoid organ of the immune system located in the thoracic cavity that serves as the site of T lymphocyte (T cell) proliferation, differentiation and maturation. The thymus is composed of distinct populations of epithelial cells localized into two histologically distinct compartments, the cortex and the medulla, which are encapsulated in mesenchyme. These distinct populations of thymic epithelial cells (TECs), together with dendritic cells, mesenchymal cells, and endothelial cells make up the thymus microenvironment. Hematopoietic progenitors enter the thymus microenvironment where they are are specified to the T cell fate. Immature thymocytes proliferate, differentiate and undergo positive and negative selection. During positive selection thymocytes gain the ability to recognize "self" or major histocompatibility complex proteins (MHC) that are distinct to the individual. Negative selection purges any T cells unable to accurately recognize MHC, which is important as it can lead to auto-reactivity [7]. T cell trafficking through these broadly defined microenvironments has been well characterized [8]. Hematopoietic precursors enter the thymus through the vasculature at the intersection of the cortical and medullary regions (cortical medullary junction) and are trafficked by molecular cues through the cortex to the medulla, and out of the thymus where they make up the diverse assemblage

of peripheral T cells [9].

In the thymus, symptoms of aging are especially prevalent in the microenvironment and manifest in TECs as a reduced capacity to proliferate and differentiate, which decreases the organ size and simultaneously diminishes its capacity to produce self-tolerant T cells [10-12]. This age-dependent loss of both mass and output is commonly referred to as thymic involution. Collectively, these symptoms lead to immunosenesence, an increased incidence of autoimmunity and a predisposition to disease and infection in aging populations[12]. However, neither molecular triggers nor the cellular and molecular mechanisms that drive involution are understood. This universal deterioration of immune function with age emphasizes the importance of addressing the current knowledge gap in understanding the shifts in cellular neighborhoods and compartment patterning that occur across the lifespan, which are vital to the successful development of regenerative therapies.

FOXN1 and Control of Thymic Epithelial Cell Differentiation and Patterning

A diverse repertoire of TFs oversees the normal development and proper function of the thymus. FOXN1 is a TEC-specific TF that is crucial to thymus fate specification, proliferation, and differentiation [13]. The necessity of *Foxn1* in thymus development is evident in Foxn1 null mice, which abort thymus organogenesis at an early stage and are functionally athymic, and therefore immune deficient [14]. *Foxn1* expression is initiated in TECs at embryonic day 11.25, and expression continues into adulthood where it is required for TEC maintenance [15,16]. The decline in *Foxn1* expression levels is an early marker for the onset of age-associated thymic involution [17,18]. The postnatal decrease

in *Foxn1* expression levels observed in aging TEC populations are mirrored in the *Foxn1*$^{z/z}$ hypomorphic mouse strain, in which *Foxn1* expression declines early at about P7 [18]. This downregulation of *Foxn1* expression levels is sufficient induce premature involution, resulting in a reduced thymus size, reduced TEC proliferation and loss of MHCII^{+}medullary TECs (mTEC) [18,19]. Additionally, *Foxn1* overexpression has been shown to retain TEC populations and reverse age-related thymic involution [20,21]. *Foxn1* expression levels change from fetal to adult stages in different TEC subsets, yet in both stages *Foxn1* influences the developmental program [18,20,22-25]. *Foxn1* modulation of both TEC proliferation and differentiation is critical during expansive embryonic stages and is required to establish thymus homeostasis in adults [13].

As FOXN1 orchestrates nearly all aspects of thymic organogenesis and homeostasis, the elucidation of potential Foxn1 targets and associated regulatory circuits is critical to understanding the process of involution and for establishing robust models of thymus regeneration. One study identified direct transcriptional targets of FXON1, using a ChIP-seq approach and a tagged Fonx1 transgene [26]. This study confirmed several suspected targets of FOXN1 in TECs, including *Dll4, CCl25,* and *Kitl.* In addition, it identified multiple elements of the cTEC and mTEC differentiation programs as direct FOXN1 targets, including β5t/Psmb11. However, how these direct targets are differentially activated in developing TECs, and how FOXN1 targets change over the course of thymus development and the postnatal lifespan, remain unknown.

Cell Cycle, Organogenesis, and the Thymus Developmental Program

The cell cycle comprises a series of highly regulated phases that result in cell

growth, DNA synthesis, and ultimately cell division. The stages of the cell cycle are divided into three phases: G_0, which is the quiescent phase; interphase, which is focused on growth and DNA synthesis; and the mitotic or M phase, when cell division occurs. Interphase is composed of three stages: Gap 1 (G_1), the first growth period; Synthesis (S), when DNA is synthesized; and Gap 2 (G_2), the second growth period and point when the cell prepares to undergo mitosis. The transition between G_1 and S is controlled by the Retinoblastoma (Rb) pathway, which blocks S phase entry and stimulates terminal differentiation through the induction of tissue-specific gene expression [27]. Rb, like many cell cycle pathways, is regulated by cyclins and cyclin-dependent kinases that phosphorylate specific proteins during distinct stages of the cell cycle. Cyclins and cyclin-dependent kinases can be activated by extrinsic signals, including a variety of growth factors [28]. During G1 cyclins D (cyclin D1, D2 and D3) and E (E1 and E2) facilitate progression from G to S phase by phosphorylating and inhibiting Rb activity [27,29]. When uninhibited the Rb genes (Rb, p107, and p130) form a repressive complex with the E2F family of transcription factors, and in doing so can regulate cell cycle progression by regulating the transcription of cell cycle E2F-dependent genes [30,31]. There are 9 known members of the E2F gene family, which are categorized as either transcriptional activators (E2F1, E2F2, E2F3a) or transcriptional repressors (E2F3b, E2F4, E2F5, E2F6, E2F7a, E2F7b [32-35]. The E2F transcriptional activators promote cell cycle but are repressed when complexed with Rb, while the transcriptional repressor E2Fs (E2F4 and E2F5) are associated with p130 and p107 regulation, suggesting that Rb gene family function is not entirely redundant [29,35-37]. In addition to the repression of the E2F gene family, Rb enlists histone deacetylase 1 (HDAC1) enzymes that induce

chromatin remodeling and further silence E2F binding sites [38,39].

Patterning of the central nervous system (CNS) requires a tightly controlled balance between differentiation and proliferation, therefore it is not surprising that a well-documented example of cell cycle regulation of differentiation has emerged from the CNS [40]. In Xenopus, the TF Neurogenin 2 (NGN2) is phosphorylated and rendered inactive by CDKs during the early stages of fetal development. When cell cycle checkpoint machinery is initiated, cell cycle length increases, allowing for the buildup of CDK inhibitors (CKI). The increase in CKIs inhibits CDK activity, which releases the inhibition on NGN2 and drives downstream gene targets that are required for differentiation [41]. There are many other examples of cell cycle regulation of development and maintenance, including the notch [42] and Wnt signaling pathways [43]. However, the notion of cell cycle regulation of thymus size is novel and warrants further exploration because regulation of postnatal thymus size is vital for maintaining a robust peripheral T cell pool and proper immune function.

Previous research has implicated the cell cycle, and specifically the Retinoblastoma (Rb) pathway, which is active during the G1 phase, as a regulator of thymus growth and differentiation [5,6]. The importance of cell cycle regulation of proliferation in TECs has been explored through an assortment of genetic perturbations. Two of these, the Rb family null mutant [5], and the K5.CyclinD1 overexpression mutant [6] strongly implicate cell cycle regulation of TECs through the Rb pathway. Rb family null mutants retain the fetal developmental program, which results in indeterminate thymus expansion, activation of E2Fs, and increased Foxn1 expression levels [5]. Complete deletion of the Rb gene family, *Mx1-Cre Rblox/lox; p130lox/lox; p107−/−*

mice**,** is lethal [44]. However, the retention of one copy of p107 (*Mx1-Cre Rblox/lox; p130lox/lox; p107+/−* or *Mx1-Cre p107-Single*) is sufficient to reverse this lethality, although these mice still have a reduced lifespan due to TEC hyperproliferation [44]. This phenotype is similar to that seen with the K5.CyclinD1 transgene, which expresses Cyclin D1 under control of the keratin 5 promoter and is expressed in epithelial cells including those in the skin and thymus [6]. Cyclin D1 is as negative regulator of the Rb pathway, and thus its expression can mimic Rb family loss of function. As with the Rb family mutant mice, K5.CyclinD1 mutants have a properly organized hyperplastic thymus, and an increase in T cell numbers but no discernable deficiencies in T cell function [6]. This increase in thymus size occurs only after about postnatal day (P)10-14. In both the *Mx1-Cre p107-Single* and the K5.CyclinD1 mutants the hyperplastic thymus phenotype is associated with up-regulation of the critical TEC transcription factor *Foxn1,* and can be rescued by a FoxN1 hypomorphic allele, $Foxn1^{z/z}$, which normalizes Foxn1 expression levels and thymus size [44]. Together, these data strongly implicate CyclinD1/Rb/E2F pathway regulation of Foxn1 expression levels as a potential regulator of thymus size, specifically at the transition from the fetal/neonatal developmental programs and the adult thymus.

Architecture of the Thymus Microenvironment

During fetal development TEC proliferation is rapid and is focused on expansion. TECs then enter a transition period and switch to an adult homeostasis phase where the emphasis becomes directed towards maintenance. In mice the neonatal transition period spans approximately postnatal day 0 to postnatal day 10 (P0-P10). During this transition

period the thymus undergoes cellular compartment reorganization [45,46] and structural changes that could extrinsically drive TEC divergence from the fetal program. These changes include differentiation of hematopoietic stem cell (HSC) populations [47] and fetal [45] and neonatal [48] structural alterations in thymic vasculature.

While developing T cells (thymocytes) are the most abundant cell type in the thymus and account for ~99% of the total cell count, thymus function depends on the remaining 1% that comprise the thymic stroma. Thymic epithelial cells (TECs) account for most of the stroma, along with contributions from fibroblasts, epithelial cells, dendritic cells, and macrophages. There are two major functional compartments in the thymus, the medulla and the cortex. The centrally located medullary compartment is encircled by the cortico-medullary junction which is surrounded by the cortex and the outermost subcapsular region. execute central and peripheral tolerance and are thus vital to generating mature T cells. TECs are divided into two major subsets, cortical (cTEC) and medullary (mTEC), based both on their location in the thymus and their molecular signatures (Figure 3.1). Both mTEC and cTEC are of endodermal origin [49], and are characterized by atypical epithelial morphologies [50].

The cortex serves as the site of positive selection. cTEC are defined by the expression of the intermediate filament protein Keratins 8 (K8) and 18, the c-type lectin CD205/Ly51, and Beta 5t /PSMB11 which comprises a portion of the cortical thymoproteosome. cTEC have a particularly distinct morphology with long looping processes that engulf developing thymocytes, with up to 100 thymocytes associated closely with each cTEC [51]. These protrusions diminish with aging [51], although it is unclear whether that is a cause or consequence of reduced cortical thymocytes. cTEC are

also the least well characterized molecularly, in large part because they are difficult to isolate from the intact organ in significant numbers. The major markers used to identify cTEC are the intermediate filament protein Keratins 8 (K8) and 18 [52], the c-type lectin CD205/Ly51 [53,54] and Beta 5t /PSMB11, a subunit of the thymus-specific proteosome [55]. Of these, K8 is the least specific, as it is also expressed at lower levels in many mTEC. There are not well characterized cTEC subsets, and they are generally considered to be a single TEC subtype, although it is unclear if that is really accurate.

mTEC appear to be more diverse than cTEC, with multiple distinct subtypes defined molecularly and functionally [56]. Morphologically, mTEC are diverse across a spectrum of shapes, rather than falling into distinct subsets, and these morphologies do not appear to change with aging [51]. Molecularly, mTEC have been traditionally been identified histologically as K5+, with additional markers K14 and the UEA-1 lectin marking distinct subsets. Functionally, mTEC are also functionally characterized by expression of CD80 and by expression of the Aire and FezF2 genes, which are required for expression of distinct subsets of self-antigens required for negative selection [57]. A lineage-restricted mTEC progenitor has also been defined by the expression of Claudin 3/4 (Cld3/4), particularly in the fetal thymus [58]. More recently, mTECs in the adult steady-state thymus have been characterized as falling into four subsets by single cell RNA-seq, defined by expression of the markers PIGR, Doublecortin, CD49, and AIRE [56] (Figure 4.1). mTEC are often also grouped into mTEClow and mTEChi subsets according to the level of MHC Class II genes (MHCII). At this point it is still unclear how all of these different characterized subsets relate to each other. Thus, mTEC diversity and delineation of the subsets both molecularly and geographically within the

medulla is clearly an area of ongoing investigation that is important for understanding thymus structure and function.

HSCs differentiate in a migratory path through the thymus microenvironment via a series of interactions with these and other stromal cell types. Postnatal HSCs migrate from the bone marrow through vasculature into the thymus [7,59] and so do not maintain a perpetual pool or niche in the thymus microenvironment [19]. During the neonatal transition period these transitory HSCs shift from a fetal program to an adult program [47]. The transition from the fetal to the adult HSC state is regulated by a decrease in Lin28 expression and a corresponding increase in let-7 expression [47]. Interestingly, during the neonatal transition period the vasculature network in the thymus reorganizes [45,60]. Vasculature in the thymus is formed from endothelial and mesenchymal cellular inputs and form a vast network of medullary localized blood vessels and cortex localized capillaries [46]. Throughout development vasculature networks are spatially linked to TEC populations and initiation, development, and maintenance of the vasculature network requires TEC differentiation [45,59]. Further investigation revealed that TEC specific *Foxn1* expression impacts the maturation of vasculature in both the fetal [45] and the neonatal thymus [60]. Previous research has shown that TEC expression of Foxn1 regulates the microenvironment in a dose dependent manner to induce vascularization in the thymus. In wild type mice endothelial cells are initially detected in the thymus at E.13.5. In $Foxn1^{\Delta/\Delta}$ and $Foxn1^{\Delta/nu}$ mice endothelial entry is delayed and in $Foxn1^{nu/nu}$ mice endothelial entry is completely undetected [45].

Vasculature at the CMJ have been identified as the site where hematopoietic precursor cells and T cells traffic in and out of the thymus and are thus a crucial

component of a functional thymic microenvironment [61-63]. As mentioned above, significant vasculature reorganization occurs when the developmental program transitions from fetal expansion to adult homeostasis stages in the early postnatal period [48], but very little is understood about how the vasculature network is patterned and regulated postnatally. However, the vast and complex 3-dimentional networks generated by vasculature make whole organ phenotypic characterization and functional testing difficult using traditional approaches.

In many organs and tissues, vasculature inputs have been shown to be bound mechanistically with nerve bundles and lymphatic inputs throughout development [64]. Potential similarities between how the blood brain barrier functions to regulate cellular trafficking in and out of the brain might offer insights into functional roles for vasculature, nerves, and the trafficking of cells in the thymus, making this an intriguing subject for future study. Lymphatic inputs have never been reported definitively or characterized in the thymus. The role of and characterization of neural inputs in the thymus has been relatively neglected for decades. Thus, there exists limited imaging and historical data about neural inputs and specifically their function in the stromal compartment of the thymus. The idea that there exists crosstalk between the central nervous system and the immune system is not however a novel concept and this notion is supported by embryonic data which demonstrated that neural crest cells are required to pattern the thymus [65,66]. Additionally, the thymus is innervated by parasympathetic and sympathetic nerve fibers of the peripheral nervous system and it has long been postulated that these neural inputs play a role in thymus function [67]. Innervation of the thymus has been shown to have derived from the superior cervical ganglion [67] and the

vagus nerve [68], and may occur as early as late in embryogenesis (E20) [69] More recent studies have localized fibers to the corticomedullary junction in close association with dendritic cells and thymocytes [70].

It is increasingly clear that the cellular milieu of the thymus is diverse and complex. Changes in the composition and organization of the resulting microenvironments are critically related to changes in thymus function over the lifespan that impact thymus function, and thus the peripheral T cell compartment and immune competency. This project was designed to address this knowledge gap by constructing a 3-D model of the structure of the postnatal thymus with specific focus on the medulla and testing how this structure changes both across the lifespan and in response to changes in FOXN1 expression levels.

CHAPTER 2

DEVELOPING AN OPTIMIZED METHOD OF TISSUE CLEARING FOR WHOLE ORGAN IMAGING

Introduction

Recent advances in high throughput single cell and FACS technologies have driven a renewed interest in the examination of whole organs, rooting single cell findings by placing them within the broader context of the intact organ. Perhaps in no field is this more evident than thymus biology, as decades of analyses following a variety of cellular disassociation techniques have yielded an abundance of quantitative molecular and cellular data, but with little or no reference to their spatial organization. A core constraint of generating whole organ multi-scale phenotypic atlases is navigating scales from subcellular, to organ-wide levels. Such needs drove the development of efficient tissue clearing pipelines that retain the spatial integrity of an organ's molecular architecture, while allowing for multiple interrogations of the same organ. The various tissue clearing technologies offer potential solutions, yet caveats such as endogenous autofluorescence, tissue dysmorphia, incomplete label penetration, and lengthy processing times continue to plague the field and adversely affect the precision and sensitivity of results. We have optimized a tissue clearing technology that minimizes these limitations; combined with improved multiplexing reagents and, our pipeline is both multiplexed (multiple labels),

and multimodal (multiple imaging techniques) allowing for the analyses of cellular and subcellular organization in intact tissues, organs and embryos.

Tissue Clearing Overview

The three-dimensional characterization of multi-scale inputs in the intact thymus will fuel insight into changes in cellular dialogs, specialized niches, and macro-anatomical inputs throughout the lifespan of the organ by localizing key transcripts and proteins, with respect to cell types, cell neighborhoods, and anatomical localizations. This permits the characterization or identification of key cell, tissue and molecular interactions that contribute to or regulate organ function, development, regeneration, and degeneration. There exists an abundance of published tissue clearing technologies and all aim to achieve deep imaging of intact tissues and embryos. The various tissue clearing technologies such as 3Disco [71], CLARITY [72], PACT [73], CUBIC [74], and PEGASUS [75] all seek to retain endogenous protein arrangement while removing light scattering lipids. For a variety of reasons such as time, ease, cost, and tissue integrity we chose to employ a modified version of the PACT tissue clearing protocol to carry out our experiments. This optimized technique integrates a hydrogel matrix within the tissue that once polymerized acts as a scaffolding to hold all DNA, RNA, and proteins in place. Pigment containing lipids are then passively removed from the tissue through extensive detergent washes rendering the tissue transparent. Cleared samples are then antibody stained and imaged [73].

For the purposes of this study this technique was modified and then used successfully to identify mTEC subtypes within spatial and temporal associations amongst

various structural inputs in wild-type, and Foxn1$^{z/z}$ mice from the neonatal time period to advanced immunosenesce (16 mos). The following antibodies were employed: medullary TECs (K14 (Biolegend, catalog # 906001 & Biolegend, Catalog # 905304), PIgr (R&D Systems, Catalog # AF2800), Aire (Millipore, catalog # 04-150) CD49 (Thermo Fisher Scientific, Catalog #, PA5-12334), doublecortin (Santa Cruz Biotechnology, Inc, Catalog number sc-271390)); vasculature (CD31(BD Biosciences, Catalog # 553370 & Cell Signaling Technology, Catalog # 35282), PDGFrβ (Santa Cruz Biotechnology Inc. Catalog # sc-374573, 958-1106), Claudin 5-488 (Thermo Fisher Scientific, Catalog # 352588)); innervation (NF (Novus Biologicals, catalog number NBP1-05219)) Claudin 3 (Invitrogen, Catalog #, 34-1700) lymphatics (Lyve-1(Invitrogen, Catalog # 14-0443-820)). Secondary antibodies utilized were as follows Alexa Fluor conjugated Donkey Anti (rat-488 (catalog # A21208), rat-594 (catalog # A21209), rabbit-647 (catalog # A31573), goat-555 (Catalog # A21432), Donkey anti-mouse Dylight-405 (Novus, Catalog # NBP1-72940) and Alexa Fluor 488-conjugated donkey anti-chicken (Jackson Immuno Research, Catalog # 703-545-155) Samples were refractive index matched in 80% glycerol. Intact organs were imaged using lightsheet fluorescent microscopy (LSFM) on an Ultramicroscope (Lavision Biotec, Bielefeld, Germany) with numerical aperture of 0.135 at 16 bit using excitation wavelengths of 488nm, 555nm, and 647nm. For higher resolution images samples were imaged (tiled z-stack 200-1000um) with a 10x objective (0. NA) on a confocal laser microscope (Zeiss 880 Oberkochen, Germany) at excitation wavelengths 405nm, 488nm, 555nm, and 647nm. Images were then rendered and analyzed using IMARIS (bitplane) image analysis software Mapping stromal compartment organization permitted the generation of a whole organ wild-type

phenotypic map of the dynamic medullary compartment in developing and aging thymi. Characterization of these ultrastructural and cell type inputs stands to offer significant insights into gene expression alterations that may be acting as regulators of or being modified themselves by TEC specific life stage transitions such as development homeostasis and involution.

Tissue Clearing Optimization

Initially we tested several clearing modalities all with varying drawbacks and degrees of success before deciding to move forward with a modified version of an aqueous clearing technology known as PACT, Passive CLARITY technique. While the various solvent and aqueous based tissue clearing technologies, all allowed for volumetric imaging of the thymus, each had limitations surrounding incomplete label penetration, endogenous autofluorescence, tissue abnormalities, and exceedingly lengthy protocols. All of these obstacles negatively affected the precision of our results. The PACT protocol became a front runner in our quest to find the best path forward because this method is relatively non-toxic, allows for multiple rounds of staining, and because the drawbacks which include tissue dysmorphia, reagent penetration, and extended processing times could be somewhat remediated. The remediation of shortcomings ease of use and the fact that no additional equipment was necessary for processing further supported our decision to move with optimizing the PACT clearing technique [76] for our studies.

The thymus is largely comprised of a heterogenous population of cells and compared to other organs such as the brain, heart and liver the thymus lacks significant

ultrastructure contributions, therefore, a “gentler” approach to clearing was needed to reduce tissue swelling and maintain endogenous protein expression. While for us the PACT protocol was the best choice for tissue clearing approaches, this protocol suffered from extended processing times surrounding clearing and antibody labeling. We postulated that these drawbacks could be at least partially remediated by using non-electrophoresis based active clearing and labeling as opposed to completely passive clearing and labeling. Our thymus optimized PACT protocol minimizes the aforementioned limitations and when combined with adjusted multiplexing labeling offers multiplexed (multiple labels), multimodal (multiple imaging techniques) volumetric imaging of the intact thymus permitting the analyses of cellular and subcellular organization.

Development of the vPACT Clearing Method

Our modifications included alterations to the types and concentrations of detergents used in the PACT protocol and the addition of vacuum pressure to enhance the passive diffusion of the clearing and protein labeling reagents. (Figure 2.1) Specifically, we included an initial clearing step that uses 4% saponin, a surfactant that interacts with and removes cholesterols and phospholipids in cell membranes, in place of the initial 8% SDS clearing step. Cholesterol molecules are large and selectively targeting them for removal especially in the outer collagen rich capsule region of the thymus allows for faster clearing and reduced tissue dysmorphia. This also allowed us to decrease the SDS concentration to 4% without sacrificing tissue clearing times, which decreased the fragility of the cleared thymus samples and allowed for fewer and shorter wash cycles.

These minor changes to the reagents resulted in faster clearing and better retention of organ integrity.

We tested two different mechanisms to facilitate the enhanced diffusion of clearing and labeling reagents through intact tissues: a histology microwave and a desiccation chamber used with an inhouse vacuum system. The microwave successfully reduced clearing times and allowed for complete antibody penetration (Figure 2.2). However, consistent equipment access made moving forward with this mechanism untenable; furthermore, it required substantial modification and optimization to the microwave operational rendering this option unlikely to be broadly useful. Using the desiccation chamber and vacuum proved to be equally effective at speeding up the clearing process (Figure 2.3) while also having the added advantage of being both accessible and reliable for this project and most labs. For these reasons we chose to process samples using the vacuum-based method. Briefly samples were incubated for 3 hours at 37^0 C in the clearing reagent and then transferred to the desiccation chamber and incubated for another 3 hours at room temperature under vacuum pressure. Samples were then incubated overnight passively at 37C. Perinatal thymi P0-P14 cleared in 12 hours adult thymi cleared in 18-24 hours. The same process was repeated over a two-day period for primary and secondary antibody labelling except that primary antibody labelling was done at 4^0 C for the passive steps and over ice for the vacuum associated steps (Figure 2.1). This modified version of PACT, vPACT, allowed for adult thymi both transgenic and wild type to be cleared overnight. Furthermore, this protocol proved successful at retaining endogenous expression of fluorescent proteins in various reporter lines while also permitting the use of traditional immunofluorescent perturbations. (Figure 2.4)

Using Vascular Autofluorescence to our Advantage

Given the prominence of vasculature and its functional importance in the thymus we chose to analyze cell types and niches within the context of the vasculature network. Autofluorescence is a phenomenon that has historically complicated immunohistochemistry-based labelling technologies in a variety of mouse tissues. The autofluorescence generated by red blood cells fluoresces across many of the excitation and emission spectra wavelengths that are typically utilized in commercially available secondary antibodies. Instead of viewing the presence of this phenomenon as a hindrance we decided to use the endogenous signal found in vasculature as a free channel as distinguishing between cell types and networks is infinitely less complicated when analyzing an entire organ. While we had success directly labelling and imaging blood vessels, we had equal success using the endogenous signal while imaging using both confocal and lightsheet microscopes (Figure 2.5). Using the endogenous chromophore as a free channel allowed us to free up a channel for increased multiplexed imaging while also accomplishing our goal of visualizing protein expression within the context of the existing vasculature networks. The optimization of the clearing pipeline and the use of endogenous fluorescence from red blood cells allowed for us to generate detailed phenotypic maps of the aging thymus offering insights into patterning, cell differentiation, and specialized niches. The in-depth phenotypic maps generated can be utilized in future studies to assess changes in cellular neighborhoods or thymus ultrastructure in a plethora of mutant mouse lines as well as during dynamic life stages or times of disease.

Figures and Legends

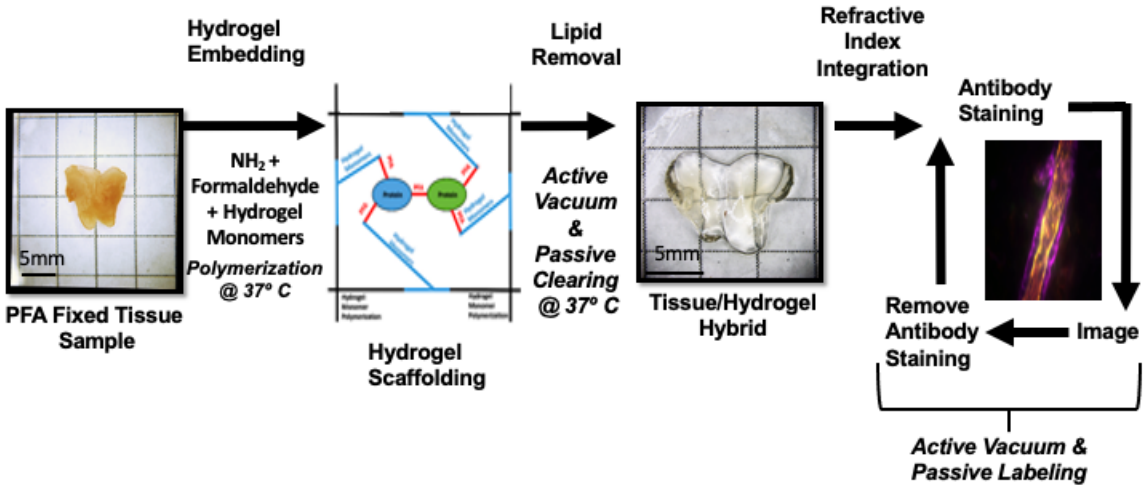

Figure 2.1: Modified vPACT Tissue Clearing Pipeline. From left, A sample is fixed in PFA overnight at 4C and then incubated in 0.025% VA-044 (thermoinitiator) and 4% acrylamide solution (acrylamide monomer solution). Incubation times vary with sample size. The tissue and acrylamide monomer solution are then polymerized at 37C. This produces a hydrogel-tissue hybrid. Lipids are then removed from the tissue using a 4% Saponin solution for 3 hours at 37C and then 3 hours in 30-minute cycles under vacuum pressure. The sample is washed and then transferred to a 4% SDS solution at 37C and cleared ON. (times may vary based on sample type). The sample is washed and then stained with primary antibodies (1:300- 1:500) 30-minute cycles (6x) are then carried out on ice in the vacuum chamber, or 4C for the passive cycles. Samples are stored in primary overnight at 4C. This is repeated for a second day. The sample is then washed and stained with secondary antibodies (1:500-1:800). Secondary staining is only one cycle (6x 30 mins vacuum and passive) over one day at room temperature. The samples are then washed a final time and refractive index matched in 80% glycerol.

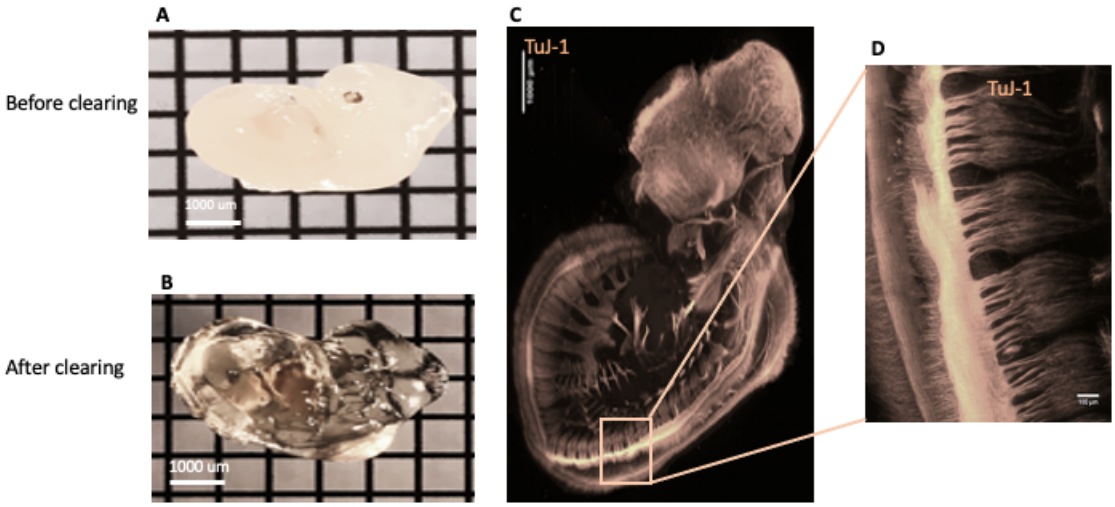

Figure 2.2: Microwave Assisted PACT. A. WT E11.5 embryo fixed and prior to tissue clearing. Scale Bar =1000um B. The same WT E11.5 embryo after microwave assisted PACT tissue clearing. Scale Bar = 1000um C. Lightsheet imaging of cleared embryo stained with TUJ-1an intermediate neurofilament marker. Scale Bar = 1000um D. Confocal 20x imaging of Tuj-1 dorsal root ganglion in the cleared E11.5 embryo. Scale Bar = 100um

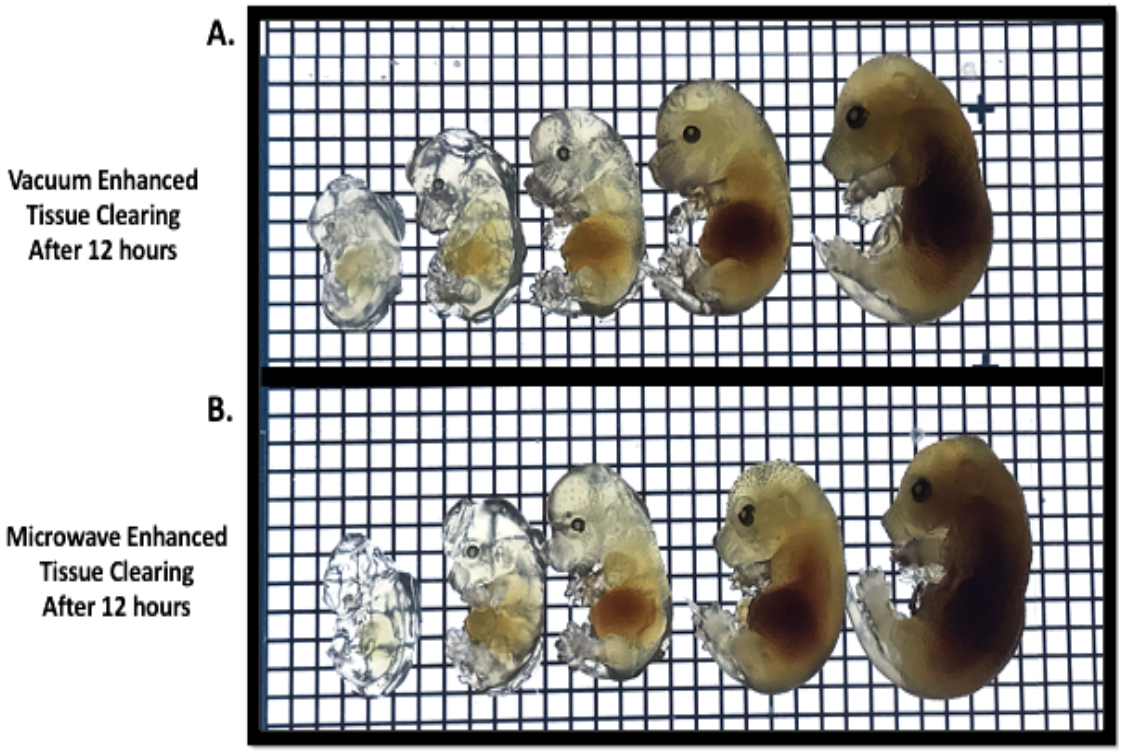

Figure 2.3 Comparison of Vacuum and Microwave Enhanced PACT Tissue Clearing. A. Embryonic time course from left to right E11.5, E12.5, E14.5, E16.5, E18.5 cleared using vacuum assisted PACT clearing for 12 hours. B. Embryonic time course from left to right E11.5, E12.5, E14.5, E16.5, E18.5 cleared using microwave assisted PACT clearing for 12 hours. Both methods are similar in terms of clearing times, tissue morphology, and tissue swelling. Each individual box on the grid is equal to $1000um^2$.

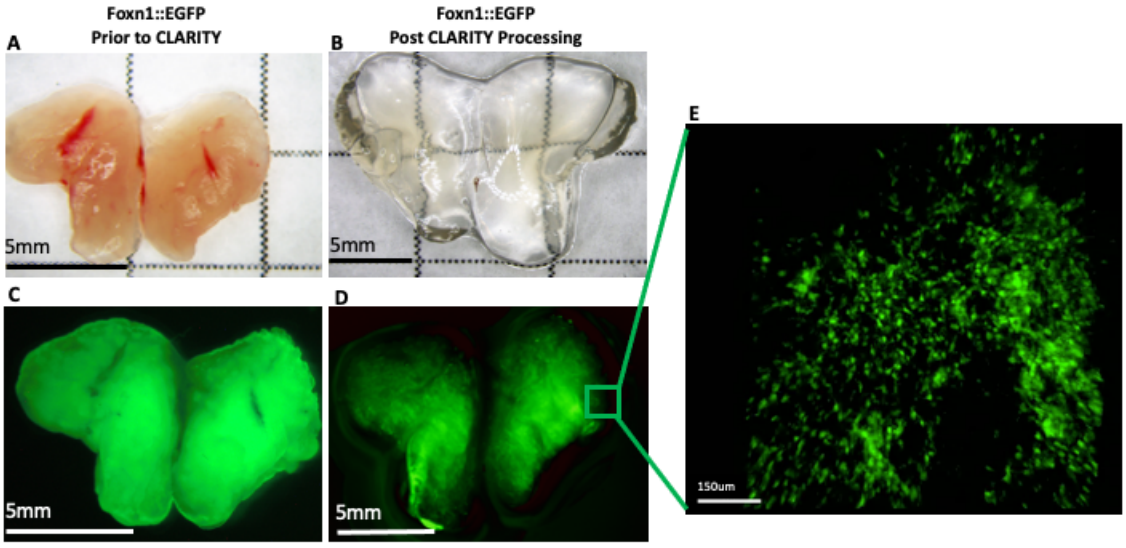

Figure 2.4: Volumetric Imaging of Cleared Foxn1::EGFP Thymus A. 5week FoxN1 EGFP thymus prior to processing. B. The same thymus post tissue clearing, now transparent. C. Low magnification fluorescent imaging shows expression of FoxN1 GFP. D. CLARITY treated thymus showing maintenance of FoxN1 GFP signal post processing with reduced autofluorescence. E. Low magnification fluorescent imaging shows expression of GFP in TECs of the FoxN1 EGFP reporter line. All samples were imaged at 10X magnification. Scale Bar = 150um.

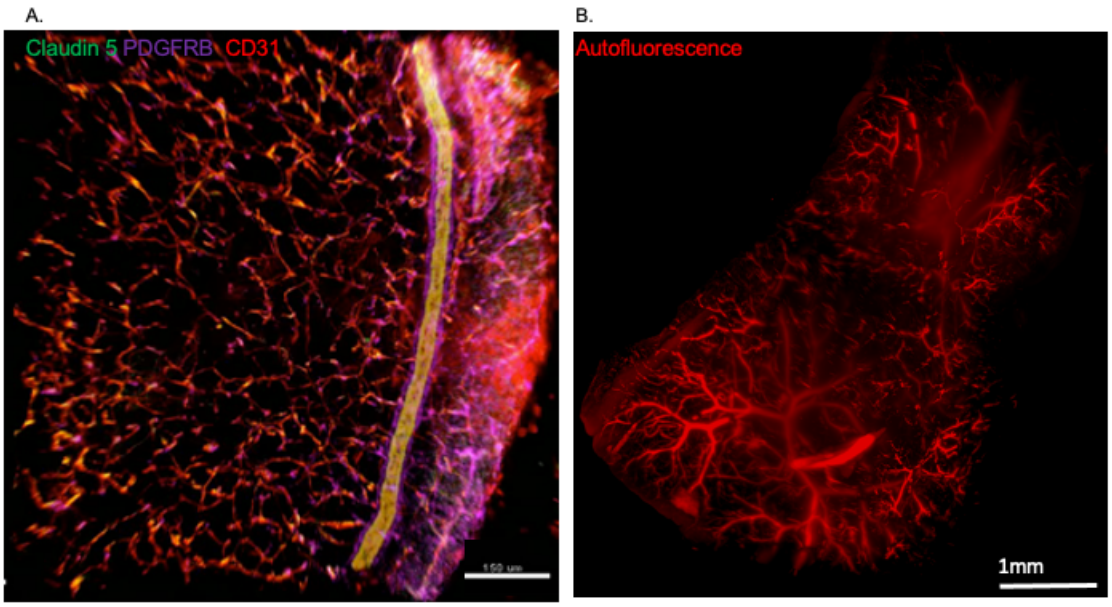

Figure 2.5 Multi-resolution Multimodal Vasculature Imaging. A.) Confocal 63X vasculature imaging of cleared P0 WT thymus stained using conventional IHC techniques with CD31a vasculature marker, PDGFrB pericyte marker, and Claudin 5 a tight junction marker. Scale Bar = 150um B.) Lightsheet 1.6X vasculature imaging of endogenous signal derived from chromophores in the red blood cells in a cleared, unprofused, 3-month-old wild-type thymus.

CHAPTER 3

A DYNAMIC MODEL OF MEDULLARY THYMIC EPITHELIAL CELL PATTERNING

Introduction

Characterizing and mapping molecular and cellular contributors to the TEC developmental homeostatic and involution programs is paramount to identifying regulators of these vastly important thymic life stages. The microenvironment is comprised of mainly TECs which are vital to T cell specification, proliferation, and differentiation. Variations in immune response can arise as a result of a variety of circumstances ranging from autoimmunity, inflammation, pregnancy, chemotherapy, inflammation and most notably aging. At the onset of involution, the effects of decreased thymic output on immune system function are minimal as T cells generated in youth a maintained in the adult. However, with aging the number of naïve T cells decline faster than they are replaced, rendering older people more susceptible to disease and secondary infections as a result of this immunodeficient state. The generation of large-scale phenotypic maps of TEC compartment changes is foundational in terms of identifying and localizing cell contributors both spatially and temporally to these dynamic alterations in thymic size and function that correspond to changes in thymic output and subsequent reduced immune response. Identifying changes in the distinct microenvironments in the thymus across the lifespan offers insights into regulatory mechanisms that underlie

thymus development, which in turn can drive the advancement of therapeutics and regenerative technologies that target the thymus's developmental clock increasing thymic output.

Nearly all efforts to understand thymus structure have used essentially 2-D approaches to visualize the organization of the thymus, based on histological and immunohistological approaches in thin sections. The overall results of these studies led to a generalized model of thymus compartment structure most often represented with a central medulla, a smooth and relatively uniform CMJ, and an outer cortex bounded by a capsule, with a designated subcapsular zone (Figure 3.1). However, this model is clearly inadequate to represent thymus structure, as even simple histology of the thymus shows that medullary structure is irregular.

While thin section approaches can offer high resolution of cellular structures and relationships, they cannot reveal the true structure of the organ. Since the thymus is not comprised of tubular structures (like the kidney or lungs) and the epithelium have an atypical morphology [51,77], it is difficult to project what the 3-D structure of the organ is based on 2-D images alone. Early efforts to render 3D models of medullary structure also showed an irregular shape for the medulla and a correlation between vasculature and medullary structure [78]. However, the lack of both markers and methods to appropriately render 3-D structure prevented any more detailed picture from emerging. We have taken advantage of the recent identification of specific markers for four medullary subsets in the postnatal thymus using scRNA-seq combined with our modified vPACT tissue clearing protocol to map the 3-D organization of the thymic medulla in the steady- state postnatal thymus. The results from this approach define new and surprising

features of the postnatal thymic microenvironment and generate new hypotheses about how thymus structure impacts function.

Results

Imaging mTEC subset localization in the 1 month thymus

To map the 3-D cellular organization of the thymic medulla, we used antibodies to label the four mTEC subsets recently identified by scRNA-seq [56] and our modified vPACT clearing method. We chose the 1-month thymus to typify the steady-state productive postnatal microenvironment. We first used lightsheet imaging to localize CD49, PIGR, and AIRE positive smTEC subsets relative to each other, and using autofluorescence to visualize vasculature in the same channel as AIRE (as thin section data had shown that AIRE+ cells are not associated with vasculature; not shown) (Figure 3.2). Lightsheet imaging allows for visualization of overall structure, but at relatively low resolution. Comparison of CD49 and PIGR mTEC subsets showed CD49 mainly lableling the deper medulla and appeared to be associated with the vasculature, while PIGR was most prominent in small discrete clusters at the outer medulla, most likely at the CMJ. Comparison of AIRE vs PIGR further reinforced this inner and outer medullary organization. This analysis presents a highly regionalized model, with AIRE restricted to the central medulla, in the region where mostly large vessels are present, CD49 in the central medulla associated with these large vessels, and PIGR largely in clusters at the CMJ.

The CMJ is characterized by PIGR+ florets

The discrete clusters of PIR at the CMJ were striking. To image these structures at higher cellular resolution, we used confocal imaging (Figure 3.4). PIGR is highly expressed and localized into clusters, with AIRE+ cells excluded and restricted to the deeper medulla as indicated by lightsheet imaging. The vasculature approaches the clusters from the central medulla and form almost a basket structure of smaller vessels (Figure 3.4A, upper left panel). CD49+ TEC are present in two distinct locations – wrapping some, but not all, of the vasculature nearing the clusters, and as individual cells in the outer region of the cluster closest to the cortex. There are also CD49+ cells in the cortex associated with the capillary bed. We will refer to the vascular-associated CD49+ TEC as sheath TEC (sTEC), and the clusters defined by PIGR expression as florets (Figure 3.2). Figure 3.5 clearly shows sTEC covering the stem region of the vasculature input that extends further into the middle of the floret defined by PIGR positive cells. Additional CD49 bright cells are located in the outer floret, not associated with vasculature.

Layering of mTEC subsets in the outer medulla

The fourth mTEC subset defined by Borenstein, et al. are defined by expression of double cortin (DC) and were identified to be similar to intestinal tuft cells [56]. To localize these cells, we used PIGR to define the florets and K14 as a broad marker of mTECs, and included Neurofilament, which labels both neuronal projections as well as a subset of mTECs and is a direct target of FOXN1 [26] (Figure 3.6A). The image in panel B gives a view of the surface of the CMJ, viewed from the side facing the cortex. This image reveals the CMJ to be composed of an irregular array of florets. Although the Z

plane has less resolution, by rotating the image you can clearly see the different medullary components that define a series of layers in the outer medulla. PIGR, DC, and NF define successive layers from the florets at the CMJ (PIGR), with DC+ cells just inside the florets, and NF+ mTECs further interior, with AIRE+ mTECs confined to the central medulla. As expected K14 is throughout the medulla, but is expressed at lower levels in PIGR, DC, and NF positive mTECs.

Loss of medullary organization and mTEC progenitors during early involution

The steady state thymus in mice spans roughly 1-2 months of age; involution begins between 2 and 3 months of age with a decline in thymocyte numbers and a decrease in *Foxn1* expression [79,80]. To assess the stability of these structures in the adult thymus during initial involution, we compared 1 and 3 month old thymi using PIGR and K14 and lightsheet imaging to define overall medullary shape and floret structure (Figure 7). At 1 month, K14 is throughout the thymus and the floret structure is clearly defined by PIGR clusters. At three months, this structure is already starting to deteriorate, with floret definition largely lost and PIGR expression scattered more uniformly across the CMJ, and some PIGR+ cells located deeper in the medulla. K14 staining is also less uniform and lower overall. This result suggests that the highly organized medullary structures in the steady-state thymus are transient and start to deteriorate rapidly with the onset of involution.

As thymic involution is essentially a loss of homeostasis, we assessed both the location of Cld3+ mTEC progenitors [58] and whether loss of these cells was occurring during early involution. Strikingly, at 1 month Cld3+ cells were also localized to the

florets, similar to PIGR (Figure 8). Both PIGR and Cld3 showed significantly decreased expression and loss of floret structures at 3 months.

Discussion

These data identify multiple new characteristics of the steady state postnatal mouse thymus. In our new model the capsule remains unchanged, but the landscape of the cortex and the medulla are significantly altered from the current model of organization. The medulla is comprised of a vast complex network of cellular structures that are only identifiable using specific markers and 3D imaging. The vascular network defines many of these key structures. The thymic vasculature enters the thymus via large arteries the enter at the midline between the two lobes, travel deep into the medulla, and then branch outward into the CMJ and then further into the cortex to establish the cortical capillary bed (non-fenestrated capillaries). These deep medullary regions with large arterial inputs in our model are called the stem region. Aire is nearly uniformly distributed throughout the central medulla, consistent with data from 2D immunohistochemistry [81]. In contrast, the other three mTEC subsets defined by Borenstein, et al, PIGR, DC, and CD49, all define new features of the medullary landscape. In addition, NF+ mTEC appear to be a novel mTEC subset, while additional K14+ mTEC are observed in all areas of the thymic medulla that appears negative for all of these subset-specific markers. Finally, these signature features of the steady-state medulla deteriorate rapidly during initial onset of involution, suggesting that they may have functional significance.

We identified two morphologically and geographically distinct types of CD49+ mTECs, the sTEC that wrap the vasculature in the central medulla and the cortical capillary bed, and the non-vasculature associated subset located at the cortical face of the florets at the CMJ. The vascular association in both the central medulla and cortical capillary bed suggests that sTECs play a role in localizing trafficking of cells into and out of the thymus, which is known to occur at the CMJ [9]. Capillaries in the cortex are also non-fenestrated (not leaky) presumably to restrict antigens roaming freely from the cortex, and these sTEC could play a role in maintaining that feature. The role of the CD49+ mTEC in the outer florets is less clear. Whether they are indeed a distinct subset, and what their function is will require further analysis.

The unique structure of the florets is striking. While the function of the PIGR+ mTECs is not known, their presence defines these florets. The CMJ has long been speculated to contain TEC progenitors, within the band of K8+K5+ TEC that are localized there [82]. The localization of Cldn3+ cells that should contain mTEC progenitors within the florets of the steady-state thymus and the loss of both Cldn3+ and PIGR+ cells and of floret organization with the onset of involution suggest that these may have functional significance. This result combined with data suggesting that mTEC cellular morphologies do not change with aging, but that mTEC proliferation declines [51], suggest that impact of involution on aging in the medulla could be changes to medullary organization and failure to replace mTECs at a homeostatic rate, and that these floret structures could maintain homeostasis.

While the Borenstein paper characterizes all mTECs in the steady-state postnatal thymus as being in one of the fours clusters identified by PIGR, CD49, DC, or AIRE, we

identified clear mTEC populations that are K14 positive but negative for these four markers, as well as NF+ TEC that have a distinct localization from these four marker-defined subsets. It is possible (even likely) that the mTEC clusters in the scRNA-seq analysis may not uniformly express these markers, and that the K14+ cells in any given region would bioinformatically be similar to the cells they are adjacent to. Alternatively, it is now well established that procedures that isolate cells from the thymic microenvironment for transcriptome or other types of analysis are highly inefficient, with most cells being lost in the process, perhaps in a non-uniform way across different TEC subsets [83]. Furthermore, clustering algorithms used for scRNA-seq datasets rely on distinct signatures of differential gene expression to define cell types. The combination of possible artifacts that can be introduced by this approach could easily result in the mis- or failed identification of subsets of cells, particularly if they are a minority population that is not easily isolated from the thymus. These data highlight the critical importance of validating data from scRNA-seq and other molecular approaches, especially those based on dissociation of the thymus into single cells before analysis, in order to understand the true implications of their conclusions.

Vasculature inputs traffic hematopoietic precursor cells and T cells in and out of the thymus and are a crucial component of a functional immune system and yet very little is understood about how the vasculature network reorganizes as the thymus ages. The vast networks generated by vasculature make whole organ phenotypic characterization and functional testing difficult. Previous research has demonstrated that vasculature inputs are bound mechanistically throughout development with nerve bundles and lymphatic inputs [64]. While it is known that the thymus is innervated [84-88], its

functional significance for thymus development, patterning, and function are not known. Organ-wide phenotypic mapping of alterations to the vasculature and neural networks is required at finer scale across the lifespan in order to elucidate functional implications of these architectural inputs. Volumetric imaging of thymic ultrastructure in the context of the dynamic post-natal medullary compartment stands to offer insights into cross-talk that underpin thymic involution.

Figures and Legends

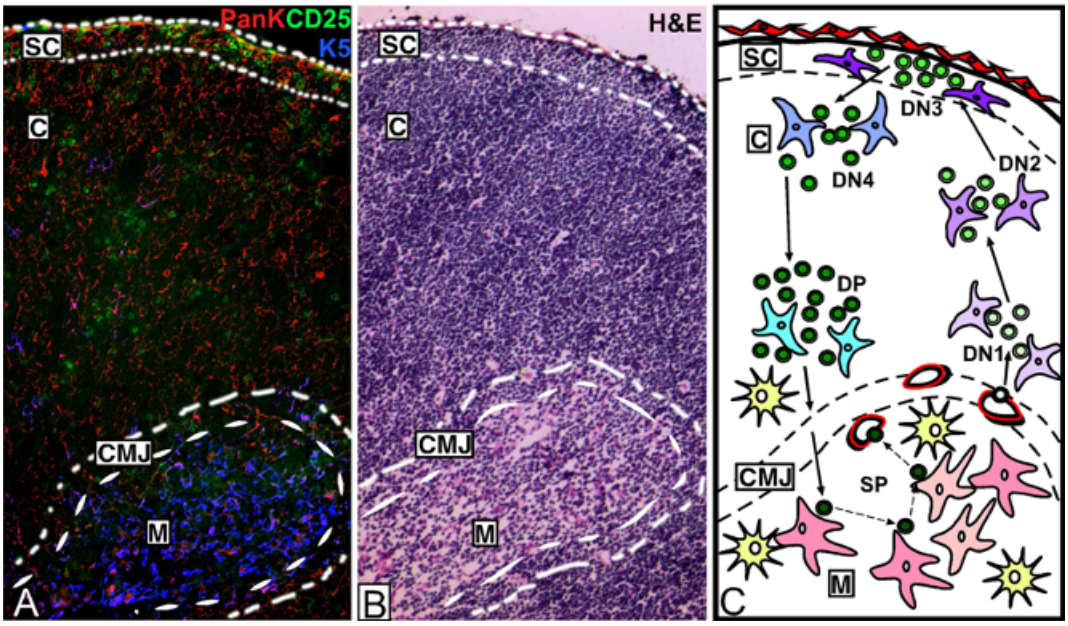

Figure 3.1: Current Model of Adult Thymus Organization. Primary thymus compartments are specified as subcapsule (SC), cortex (C), corticomedullary junction (CMJ) and medulla (M) with mTECs and cTECs confined to their respective compartments. B. corresponding H&E staining. C. Graphical depiction of T cell migration and maturation through the medulla and cortex.

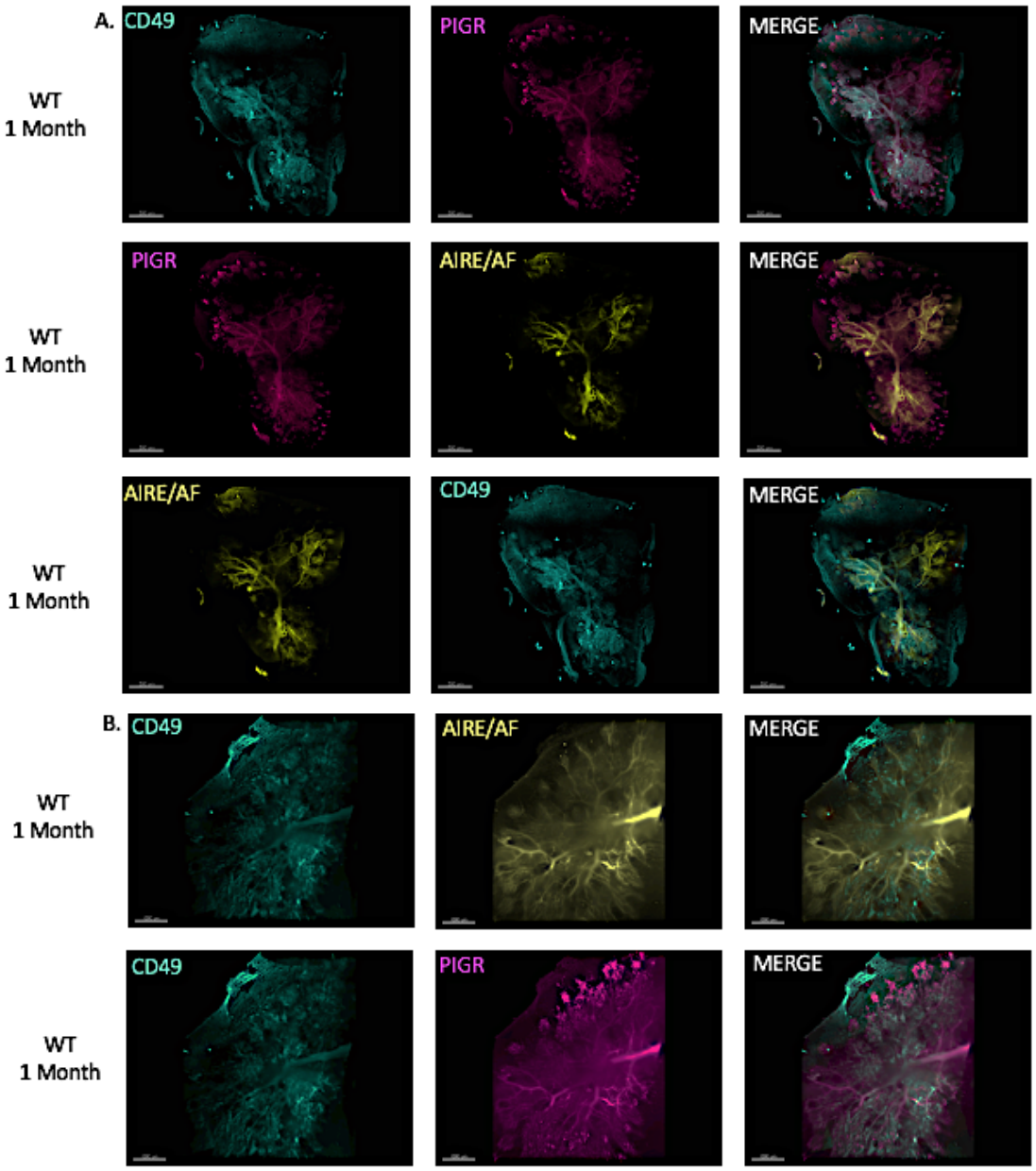

Figure 3.2: mTEC Compartment Organization. A. Lightsheet imaging (1.6X) of WT 1 month old thymic lobe. N=4 B. Scale Bar = 1500um Lightsheet imaging (2.5X) of WT 1 month old thymic lobe. Scale Bar = 1000um N=4. Each row shows pairwise combinations of the same thymus stained with AIRE (yellow, the same channel as autofluorescence from the vasculature network), PIGR (magenta), and CD49 (turquoise).

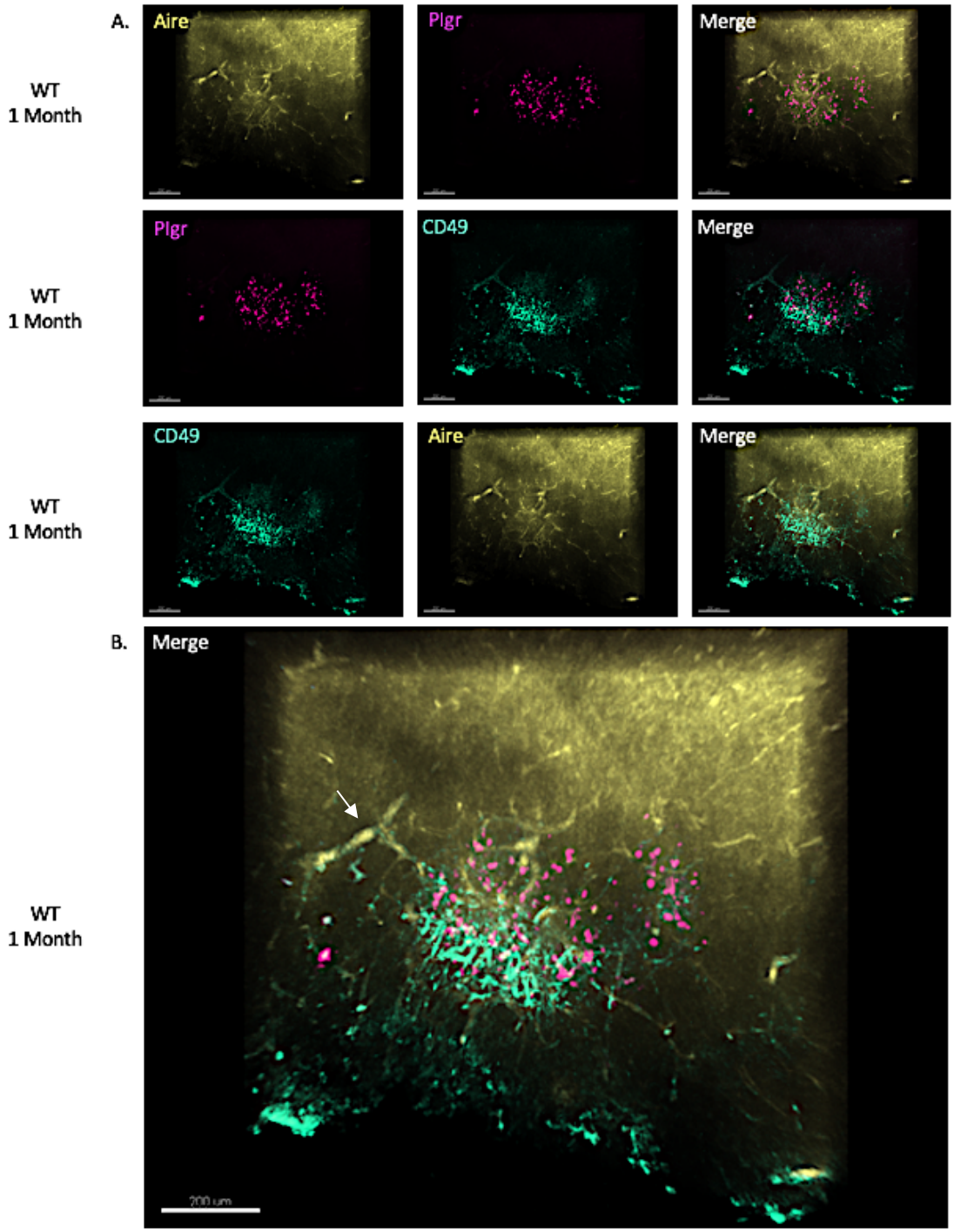

Figure 3.3: mTEC Floret Organization. A. Confocal imaging (10X) of WT 1 month old intact thymic lobe. N=4 B. Confocal imaging (10X) of WT 1 month old thymic lobe. N=4. A. Each row shows pairwise combinations of the same thymus stained with AIRE (yellow, the same channel as autofluorescence from the vasculature network), PIGR

(magenta), and CD49 (turquoise). Scale Bar = 200um B. Merge of all three markers. Arrow indicates CD49+ mTECs (sTEC) wrapping vasculature network prior to entering the floret. Dotted line indicates inner medulla where Aire+ cells and larger vessels are present. Scale Bar = 200um.

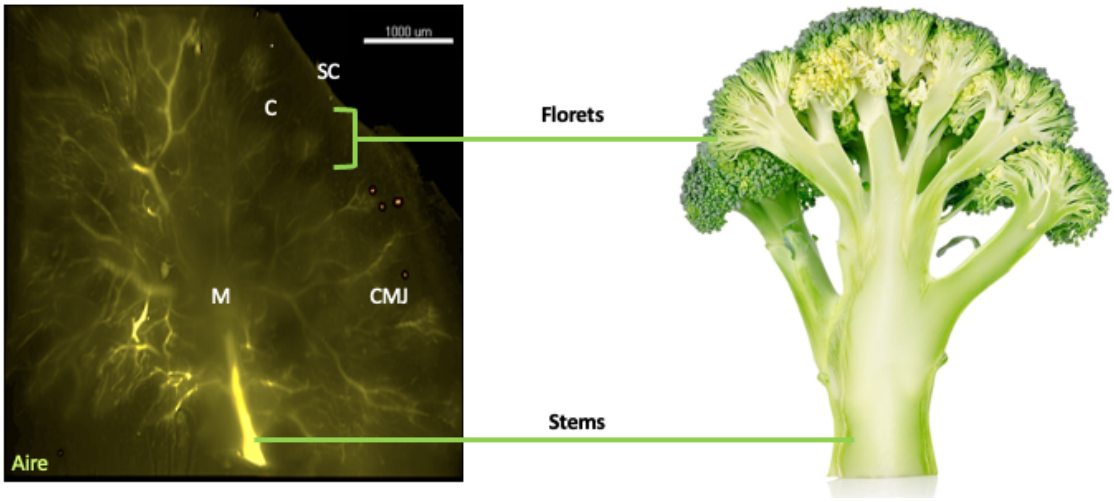

Figure 3.4: Proposed Model of Medullary Organization. (Left) Principal thymus compartments are specified as subcapsule (SC), cortex (C), corticomedullary junction (CMJ) and medulla (M). New geographical feature highlighted as Florets located at the CMJ, and Stems which are large vessels in the deep medulla 1.6X lightsheet imaging of AIRE stained WT 1month thymus. Scale Bar = 1000um

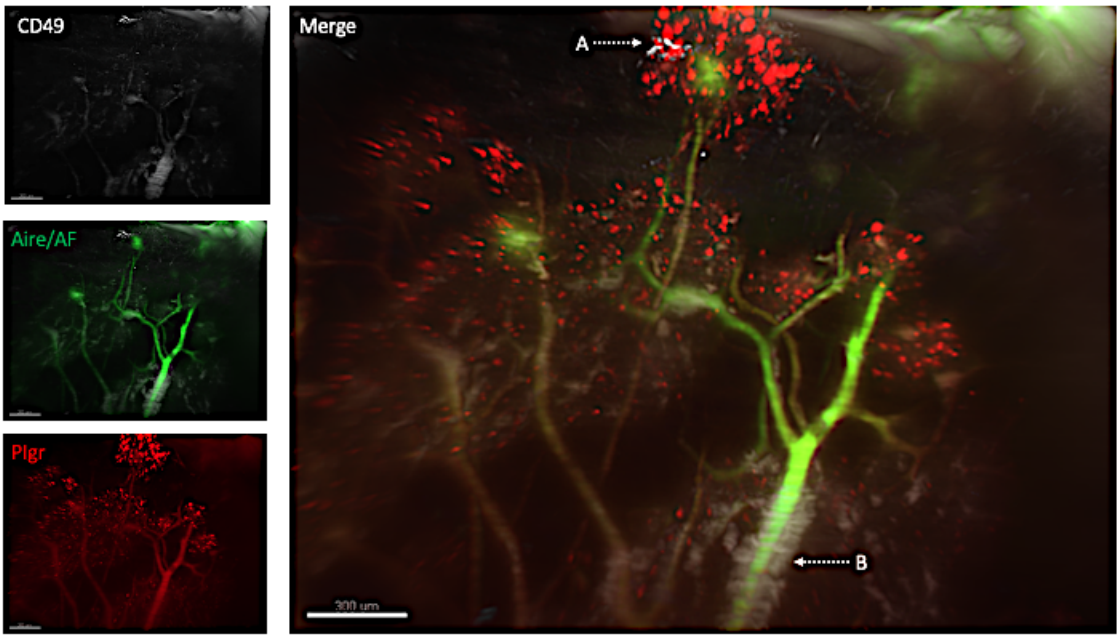

Figure 3.5: sTEC Organization in Stems and Florets. A. Confocal imaging (10X) of WT 1 month old intact thymic lobe. N=4 B. Lightsheet imaging (10X) of WT 1 month old thymic lobe. N=4. Samples stained with AIRE (yellow, the same channel as autofluorescence from the vasculature network), PIGR (magenta), and CD49 (turquoise). "A" arrow indicates CD49+ cells not associated with vasculature in the outer floret. "B" arrow indicates CD49+ mTECs (sTEC) wrapping vasculature network prior to where vessels enter the floret. Scale Bar = 300um

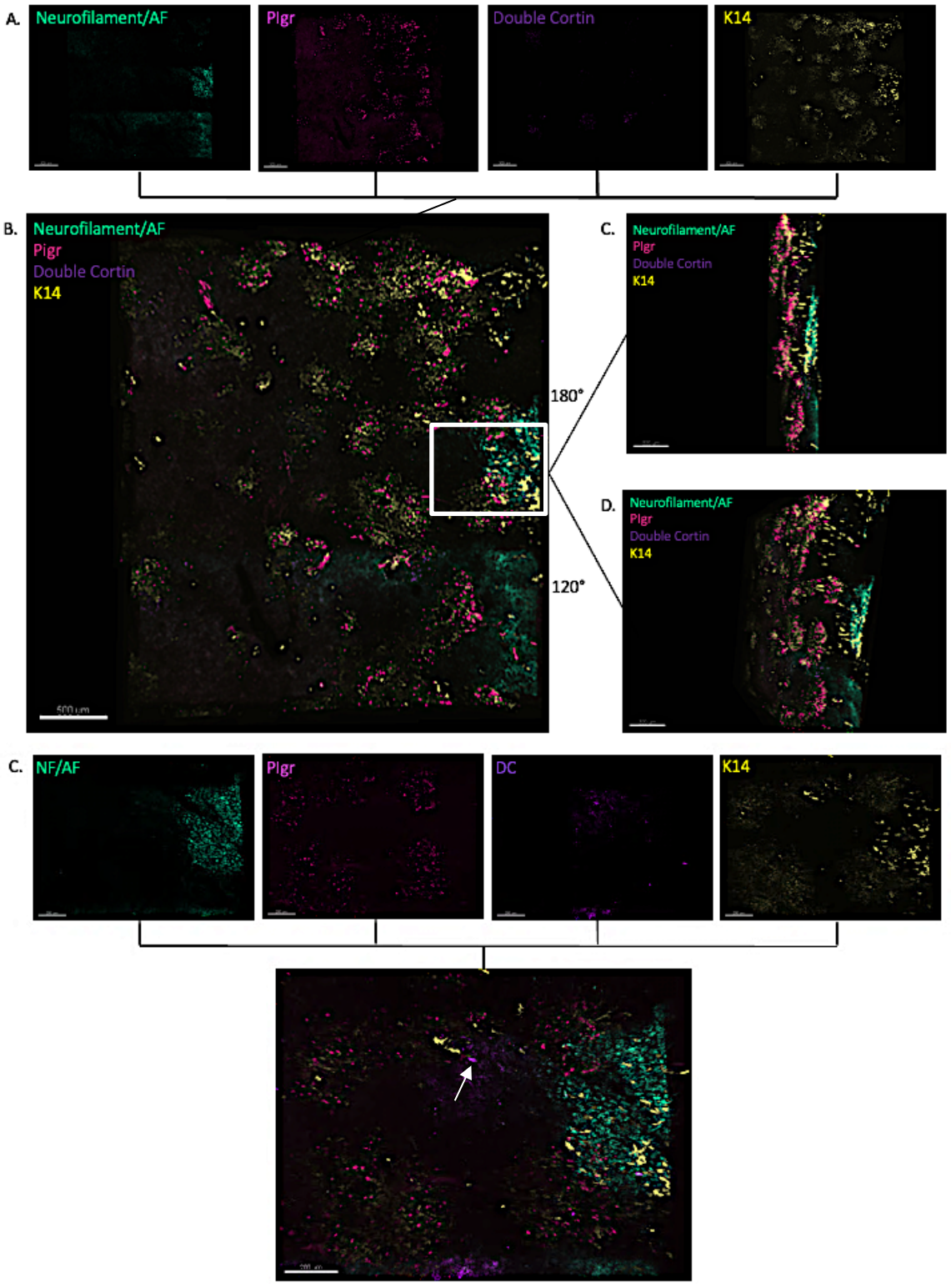
A.
Neurofilament/AF
Pigr
Double Cortin
K14
B.
Neurofilament/AF
Pigr
Double Cortin
K14
500 µm
180°
120°
C.
Neurofilament/AF
Pigr
Double Cortin
K14
D.
Neurofilament/AF
Pigr
Double Cortin
K14
C.
NF/AF
Pigr
DC
K14

Figure 3.6: mTEC Subset Layering in the Outer Medulla. A. 1 month old WT cleared thymus stained with Neurofilament (NF) in the same channel as autoflourescent vasculature (AF) (aqua), PIGR (Magenta), Double Cortin (purple), and K14 (yellow). B. Merged image. C. Merged volume rotated 180 to show layering of mTEC subsets in the medullary compartment. D. Merge volume rotated 120 to highlight that doublecortin+ cells (arrow) are present in a layer between the PIGR+ florets and NF+ mTECs. Scale Bar = 500um.

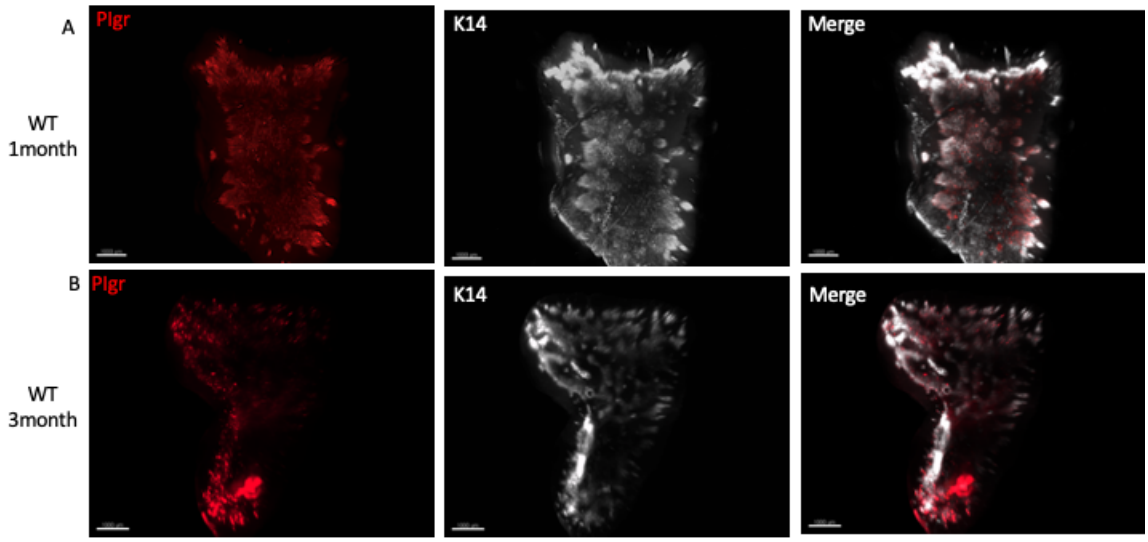

Figure 3.7: Loss of K14 and PIGR Expressing mTECs During Early Involution. PIGR (red) and K14 (white) staining at 1 month (A) and 3 months (B). Both markers are reduced in 3 months compared to 1 month, with sparser K14 and PIGR not well organized into discrete florets. N=4. Scale bar = 1000um

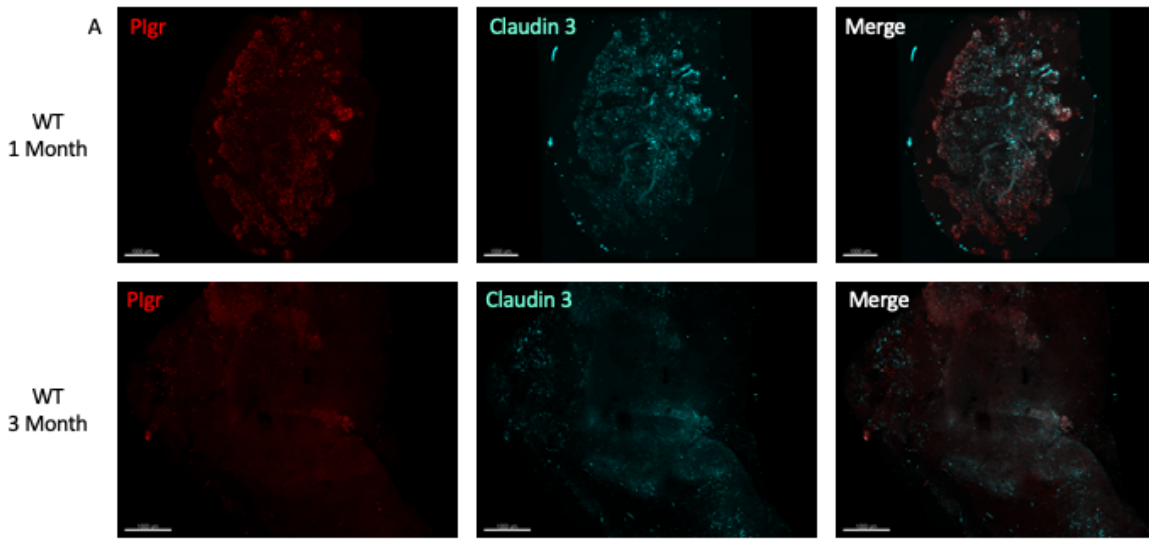

Figure 3.8 Loss of PIGR and Cld3 Expression. PIGR (red) and Cld3 (turquoise) staining at 1 month (A) and 3 months (B). Both markers are reduced in 3 months compared to 1 month. N=4. Scale bar = 1000

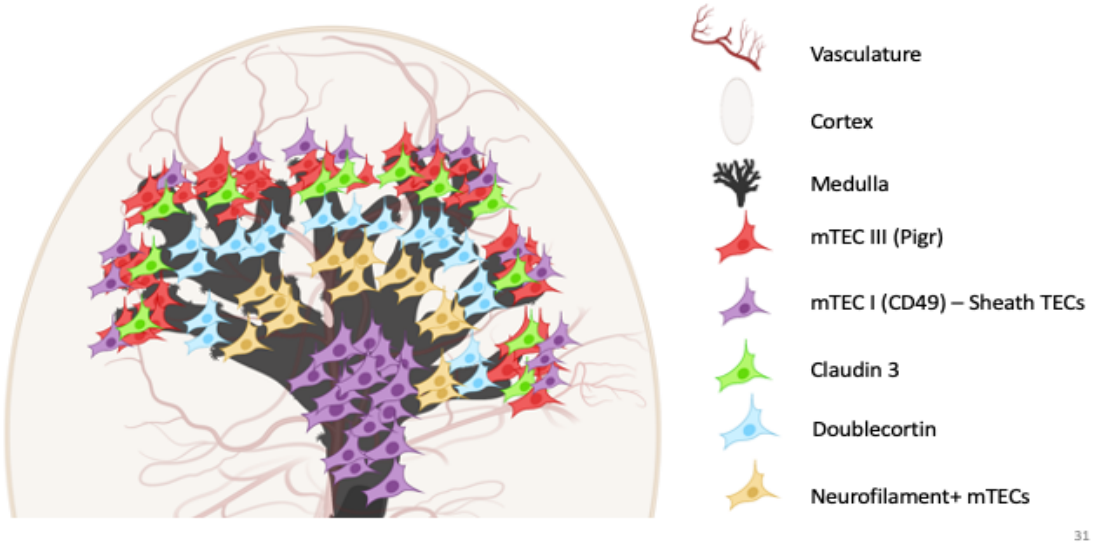

Figure 3.9: Floret Model of mTEC Patterning. Graphical depiction of steady-state medullary compartment patterning in the 1 month wild-type thymus. Created with biorender.com

CHAPTER 4

FUNCTIONAL IMPLICATIONS OF mTEC FLORET ORGANIZATION

Introduction

The surprising complexity and level of organization of our new model of the architecture of the postnatal steady-state thymus is well beyond what was previously appreciated and raises many questions about the development and functional significance of these structures. To further explore this new model, we extended our time course to include the neonatal and early postnatal thymus. The perinatal period is known to be a period of transition in the thymus, with significant functional and structural changes in the vasculature [45], the transition from fetal to adult type hematopoietic cells [47], and the transition from fetal expansion to adult homeostasis. This latter transition is controlled by the action of the Rb pathway, which suppresses TEC proliferation to establish homeostasis beginning at around postnatal day 10 (P10) [5,6]. This function for Rb is mediated by its regulation of *Foxn1* gene expression, through the action of E2F transcription factors [5]. As many if not most aspects of TEC differentiation rely on FOXN1 function, this significant change in *Foxn1* gene expression control implicates FOXN1 function as a key aspect of this transition. Furthermore, the appearance of most of the mTEC subsets that define the unique architecture of the steady state thymus in our new model occurs at or soon after this same transition point in the postnatal thymus.

Thus, it would be an obvious hypothesis that FOXN1 may control some or all aspects of this steady-state thymus medullary model.

To define the ontogeny of these features of the postnatal thymus we analyzed the expression, localization, and organization of these mTEC subsets and the vasculature in the neonatal thymus at P0, and at P7 and P14 across the transition from perinatal to adult phenotypes in the wild-type thymus. To test the role of FOXN1 in these processes, we used the *Foxn1*$^{Z/Z}$ strain, a postnatal-specific hypomorphic allele in which *Foxn1* expression is normal throughout the fetal period, but declines soon after birth [89]. Comparison of age-matched wild-type and *Foxn1*$^{Z/Z}$ mutants showed striking differences in both the expression of these subset-specific markers and in their localization and organization throughout the perinatal period, including premature differentiation and failure of floret formation. These data show that FOXN1 controls multiple aspects of mTEC differentiation and compartment organization, and further suggests that FOXN1 function serves to delay the timing of the transition from perinatal to adult microenvironments, which may be necessary to enable the generation of perinatal-specific T cell subsets.

Results

Early Cluster Organization in WT and Foxn1$^{z/z}$ *Postnatal Thymi*

To investigate the ontogeny of the medullary structures we observed in the one month thymus, we focused our attention on the perinatal transition that occurs at around P10. The wild-type thymus at P7 just prior to this transition displays what appears to be early floret organization, with clusters of cells expressing these medullary markers

(Figure 4.1A). Surprisingly, most cells in these clusters appear to be expressing multiple mTEC markers (arrows, Figure 4.1A & Figure 4.2), and some clusters include cells that are positive for only AIRE, which were not observed in the florets in the one month thymus. The layered structures of the one month medulla are not yet evident either within the florets or more broadly in the outer medulla, although DC+ thymic tuft cells are relatively few in number and are localized away from the clusters, similar to our data on their localization at 1 month. In the cortex, CD49+ sTEC are already associated with the capillary network.

The medullary compartment of P7 *Foxn1*$^{z/z}$ thymi have also started to display what appears to be early floret formation. However, in the *Foxn1*$^{z/z}$ early florets are more loosely clustered and appear to be comprised of distinct mTEC subsets including individual Aire, CD49, and PIGR cells, with few of the co-expressing cells seen in the wild-type thymus (Figure 4.1B, arrows). DC+ mTEC and cortical CD49+ cells appear similar in the wild-type and mutant thymi, although the DC+ cells are few in number in both genotypes. These data suggest that mTEC differentiation and floret formation are altered in the *Foxn1*$^{Z/Z}$ mutants, and may display premature mTEC differentiation, at least for PIGR+ and AIRE+ subsets.

Late Postnatal Floret Organization in WT and Foxn1$^{z/z}$ *Thymi*

At P14, the wild-type thymi display PIGR single positive cells localized to the CMJ, and AIRE+ cells are no longer localized to the florets (Figure 4.3). In the wild-type P14 thymus there is also the beginnings of organization of the cortical facing CD49+ TECs in the florets, suggesting the florets are dynamically patterning during this time.

The *Foxn1*$^{Z/Z}$ mutant thymus has numerous differences in organization and patterning. PIGR+ cells are more scattered in *Foxn1*$^{Z/Z}$ mutants, and PIGR expression per cell appears to be more intense in the Foxn1$^{z/z}$ mutants (both wild-type and *Foxn1*$^{Z/Z}$ mutant images were obtained using the same imaging and processing parameters). Interestingly CD49+ mTEC subsets in Foxn1$^{z/z}$ seem to be highly disorganized and are mislocalized in the outer thymus along with some DC+ cells.

Neonatal medullary organization is disrupted in Foxn1 $^{z/z}$ *mutants*

Given the intriguing patterning of early floret formation in the wild-type at P7, we investigated the structure of the P0 thymus (Figure 4.4A, C). As the medullary markers that define later mTEC subsets are for the most part not yet expressed at this stage [90], we first used K14 for mTECs, NF for both mTECs and neural inputs, and included CD31 to specifically mark the vasculature. We also used Lyve-1 to investigate whether lymphatics are present in the neonatal thymus. K14 is present throughout the medulla and defines its overall shape. The vasculature in the wild-type thymus at this stage is well developed and displays the central large vessels and branching patterns in the medulla reminiscent of that seen at later stages. Lymphatics are present, although sparse, and primarily in the medulla. NF+ mTEC clusters are abundant, as are neural fibers (although they are somewhat obscured by the clusters in this image).

We did not expect to see differences I the *Foxn1*$^{Z/Z}$ thymus at the neonatal stage, as our original analysis of these mutants indicated that *Foxn1* expression is similar to wild type until P7 [89]. However, we saw striking changes in the mutant neonatal thymus (Figure 4.3B, D). K14 is highly expressed and the K14+ medullary region is patchier and sparser compared to wild-type. There is a loss of deep medullary large vasculature, and

absence of lymphatics in the mutant. No NF+ positive clusters are observed, although NF+ neural projections are present. As NF has been identified as a direct target of FOXN1[26], its absence in mTECs at this stage suggests that the *Foxn1*^{Z} allele may have earlier impacts on *Foxn1* expression and thymus phenotypes than our previous characterization indicated.

NF+ mTECs may prepattern floret formation during the perinatal period

The presence of what appear to be NF+ mTEC clusters in the neonatal WT thymus well prior to the appearance of PIGR+ mTEC suggested that these NF+ clusters could be an early component of medullary patterning. Thus, we revisited the P7 stage, staining with both NF and PIGR (Figure 4.5). In the wild-type thymus at P7, the small discrete PIGR+ clusters are adjacent to NF+ mTEC clusters, similar to what was seen in the one month thymus. The neurite network is also extensive, and within the thymus appears to track with vasculature.

In the *Foxn1*$^{Z/Z}$ mutants at P7, as described above PIGR+ cells are present and numerous, but not as well organized into discrete clusters as in the wild-type thymus at this stage (Figure 4.6). There is little NF expression in mTECs, similar to the P0 mutant thymus. Strikingly, neurites are also quite sparse, even fewer than in the P0 thymus in the mutants. These data are consistent with a model in which FOXN1-dependent NF expression in mTECs at the neonatal stage is required to pre-pattern later floret formation at the perinatal to adult transition.

Discussion

In vivo fate mapping experiments conducted on the four recently described classes of mTEC (I-IV) revealed that mTEC IV DC+ cells are either derived from or share a common ancestor with mTEC classes II (PIGR+) and III (AIRE+). Interestingly, mTEC class I (sTECs) do not share a lineage with the other 3 classes of medullary TECs [56]. The authors of this study thus concluded that both PIGR+ and DC+ cells represent 'post-AIRE' mTEC subsets. As AIRE+ mTEC are considered to be mature functional mTEC, this conclusion would implicate both PIGR+ and DC+ tuft mTECs as very late stages of mTEC differentiation. However, our data at P7 showing extensive co-expression of PIGR and AIRE would suggest that this fate mapping could instead reflect an early transient stage of mTEC differentiation in which these markers are co-expressed, rather than a lineal maturation relationship. The distinct geographical localization of these mTEC subsets in the one month thymus also does not obviously match a lineal relationship model, except for the DC+ tuft cells being located just beneath the PIGR+ cells in the florets. The dynamic nature of these structures over a relatively short timeframe suggests that a much closer time course across the perinatal period will be needed to map the differentiation of mTEC subsets and the process by which both the florets and layered structures of the medulla form.

We expected to see variations in TEC differentiation, compartment organization and vasculature (specifically capillary density) between wild-type and *Foxn1*$^{z/z}$ mutants after P7, because TEC differentiation and vasculature organization are linked in a dose dependent manner to *Foxn1* expression [45]. However, the clear phenotypes observed at the P0 time point is intriguing as it suggests that *Foxn1* expression levels might differ

earlier than previously defined [89] This could be due to genetic drift in this line, which has been maintained in the Manley lab for over 15 years. Alternatively, as our previous analysis of this line was performed using a bulk expression approach, it is possible that down regulation of *Foxn1* from this allele could occur earlier in specific TEC subsets. An in-depth analysis of *Foxn1* expression levels in the $Foxn1^{Z}$ allele across the postnatal time course is necessary to distinguish the molecular basis for these observed earlier phenotypes. As this time frame also encompasses the fetal to adult transition in thymic microenvironments, this analysis could also yield important information contributing to the mechanisms underlying this important functional transition.

Lymphatic and neural inputs to the thymus have not been previously reported in detail, and lymphatics in particular have never been reported or characterized in the thymus to our knowledge. Our data show lymphatic inputs in close association with vasculature inputs in the P0 thymus. While innervation of the thymus has been previously reported to start, our data show an earlier innervation even at P0, and the loss of neurites in the P7 $Foxn1^{Z/Z}$ mutants suggests their maintenance might be linked to TEC phenotypes. Both of these observations suggest that further mapping and functional investigation of these novel aspects of the thymic microenvironment are warranted.

Figures and Legends

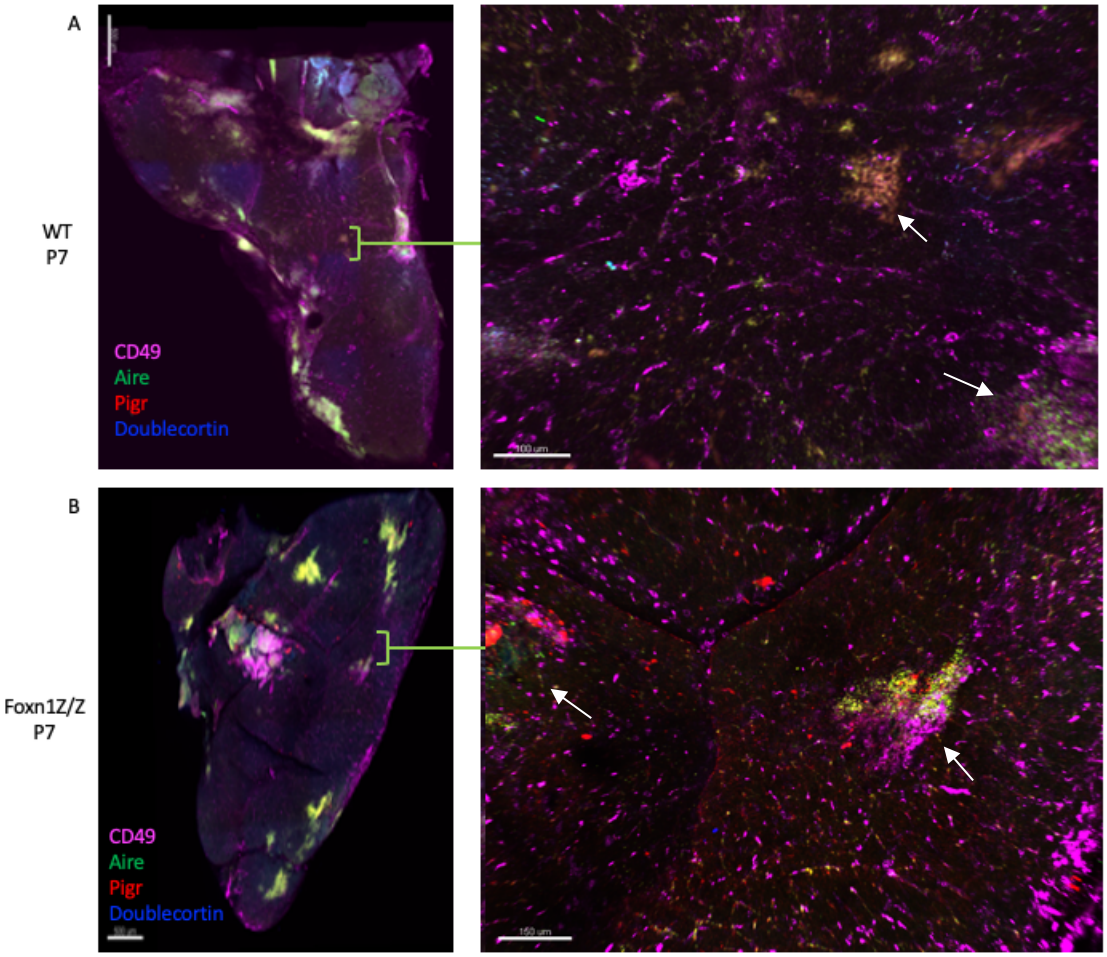

Figure 4.1: Early Floret Organization in WT and Foxn1$^{z/z}$ Postnatal Thymi A. Confocal Imaging (10X) of WT P7 thymic lobe. Scale Bar = 500um (left) 100um (right)_ N=4 B. Confocal imaging (10x) of Fozn1$^{z/z}$ P7 thymic lobe. Scale Bar = 500um (left) 150um (right)_N=4. Thymi are stained with AIRE (green, the same channel as autofluorescence from the vasculature network), PIGR (red), Doublecortin (blue) and CD49 (magenta). Arrows mark likely early florets clusters in the postnatal thymus.

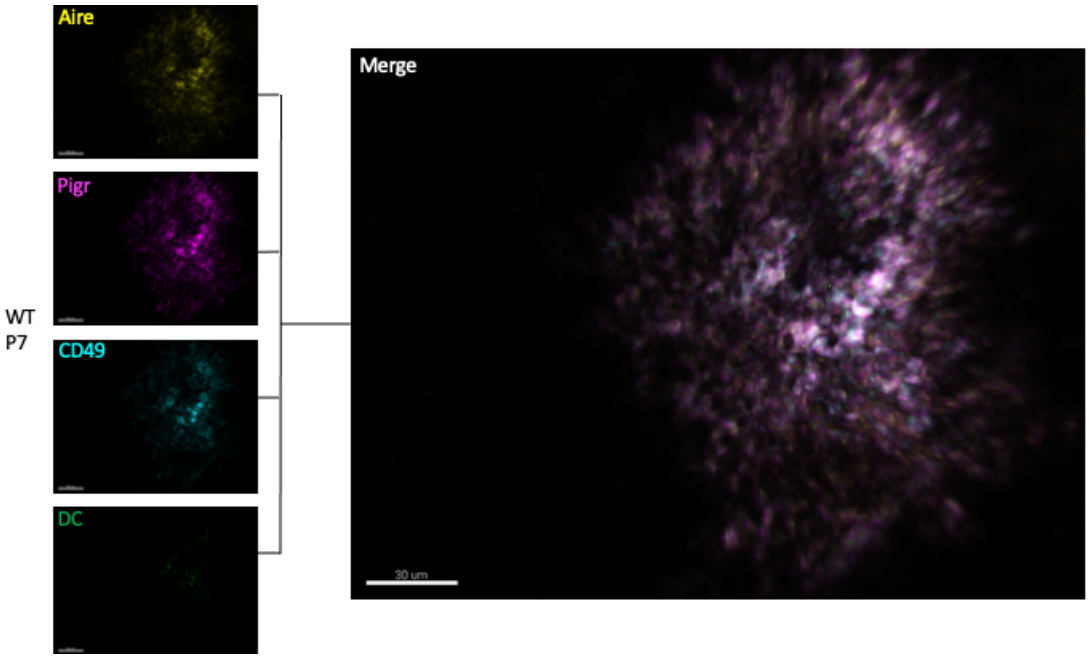

Figure 4.2: Wild-Type Early Floret Coexpression Pattern. Digitally zoomed image (Confocal 10X) of WT P7 thymic lobe. N=4 Thymi are stained with AIRE (yellow, the same channel as autofluorescence from the vasculature network), PIGR (magenta), CD49 (turquoise) and Doublecortin (green). Scale bar = 30um.

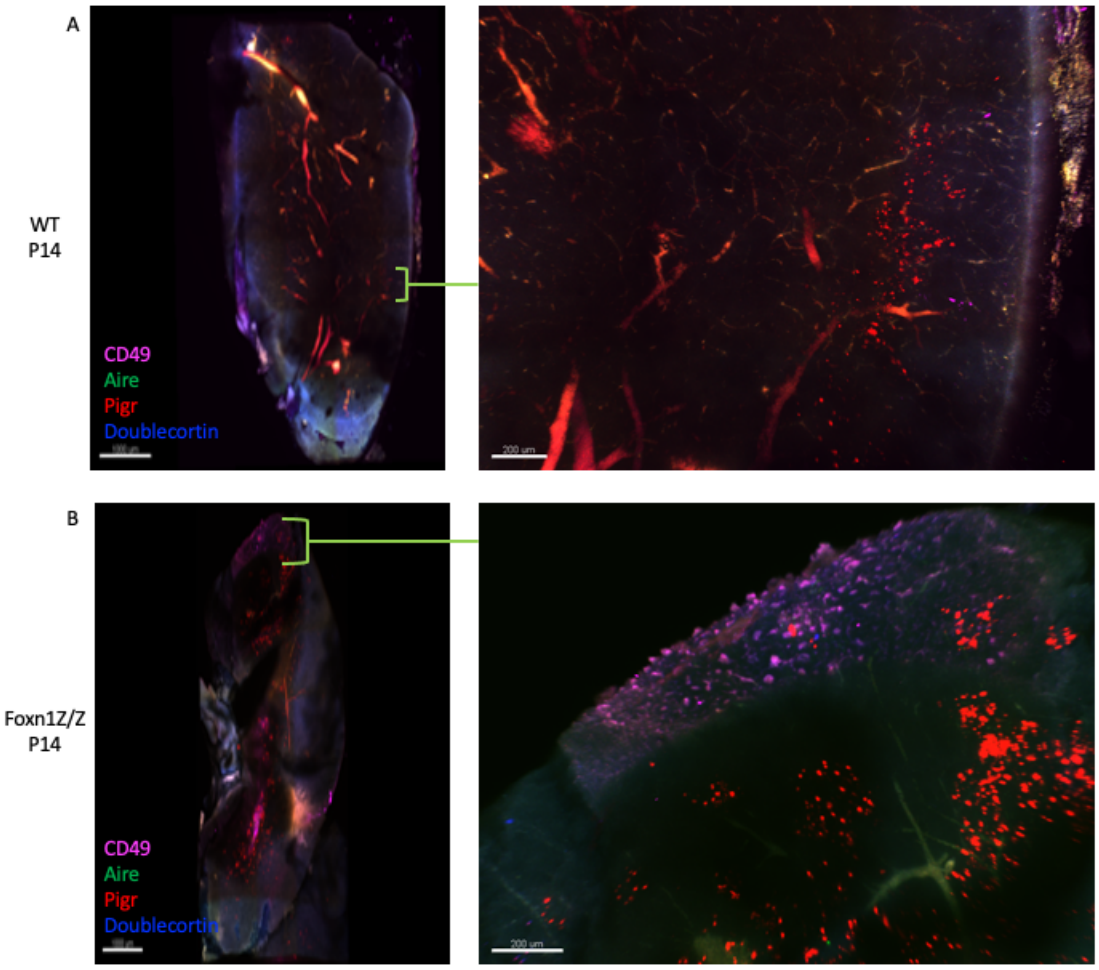

Figure 4.3: Late Postnatal Floret Organization in WT and Foxn1$^{z/z}$ Thymi A. Confocal Imaging (10X) of WT P14 thymic lobe. Scale bar = 1000um (left) 200um (right) N=3 B. Confocal imaging (10x) of Fozn1$^{z/z}$ P14 thymic lobe. Scale bar = 1000um (left) 200um (right) N=2. Thymi are stained with AIRE (green, the same channel as autofluorescence from the vasculature network), PIGR (red), Doublecortin (blue) and CD49 (magenta).

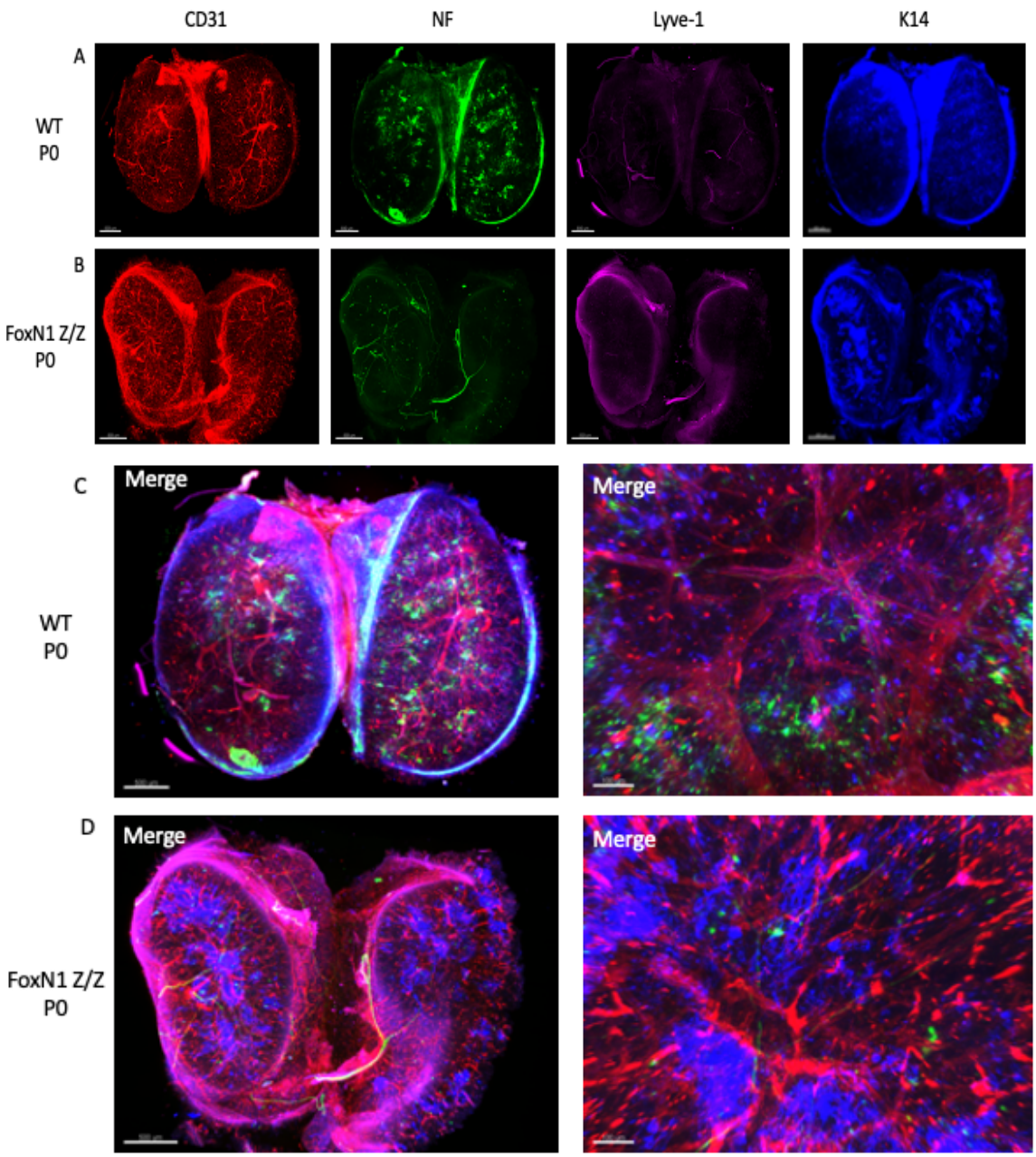

Figure 4.4: Neonatal Medullary and Ultrastructure Organization in WT and Foxn1 $^{z/z}$ thymi. A. Confocal Imaging (20X) of WT P0 thymic lobe. N=2 Scale Bars = 500um B. Confocal imaging (20x) of Fozn1$^{z/z}$ P0 thymic lobe. N=1. Scale bars = 500um C. Low magnification LSFM imaging of WT intact lobes. Scale bar = 1000um (left). Digitally zoomed. Scale bar = 100um (right). C. Low magnification LSFM imaging of Foxn1 $^{z/z}$ intact lobes. Scale bar = 1000um (left). Digitally zoomed. Scale bar = 100um (right).

Thymi are stained with NF (green, the same channel as autofluorescence from the vasculature network), CD31 (red), K14 (blue) and Lyve-1 (magenta).

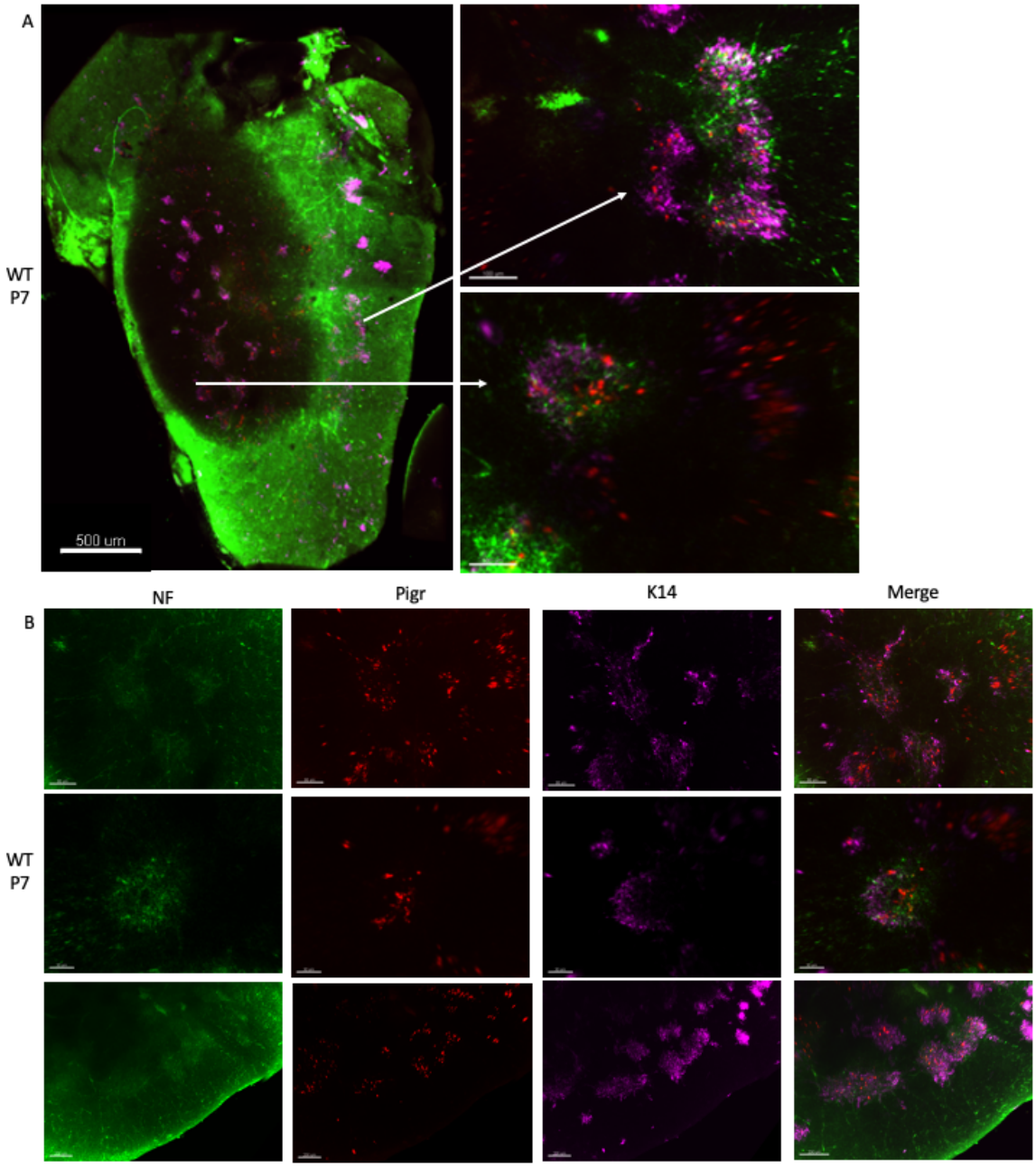

Figure 4.5: Wild-Type Innervation of Nascent Floret Clusters. A. Confocal Imaging (10X) of WT P7 thymic lobe. N=4 Scale bar = 500um (left). Digital zoom. Scale bar

=100um (top and bottom right) B. Digital zoom of early floret clusters in WT P7 mice. Scale bar = 80um (top row), 30um (middle row), and 200um (bottom row). Each row shows stainging (left to right) Neurofilament (green) PIGR (red) K14 (magenta)

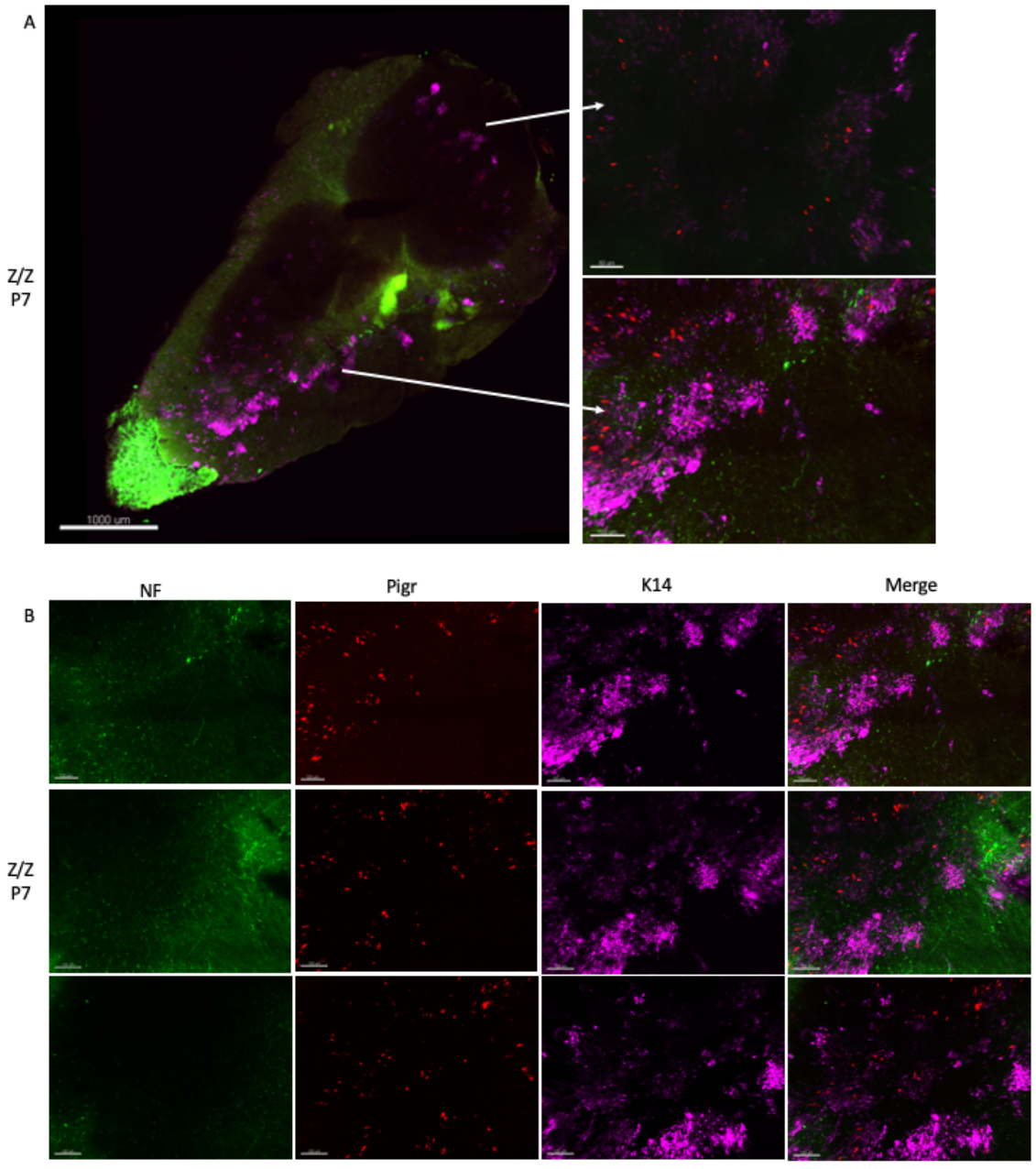

Figure 4.6: *Foxn1*$^{z/z}$ Innervation of Nascent Floret Clusters. A. Confocal Imaging (10X) of *Foxn1*$^{z/z}$ P7 thymic lobe. Scale bar = 500um (left), 50um (top right), and 100um (bottom right) N=4 B. Digital zoom of early floret clusters in *Foxn1*$^{z/z}$ P7 mice. Scale bar = 100um (top, middle, and bottom rows) Each row shows staining (left to right) Neurofilament (green) PIGR (red) K14 (magenta)

CHAPTER 5

DISCUSSION

Discussion and Conclusions

This body of work highlights the importance of taking molecular and cellular insights gained from single cell transcriptome data and placing them back within the context of the intact organ. The complex and dynamic spatial organization of these markers across developmental time offers insights into both ontogeny and patterning that are lost when cells are isolated and characterized independent of their spatial organization. Using a multiplex 3D imaging approach, we have identified the following new features and characteristics of the postnatal thymus microenvironment:

In the steady-state thymus (1-month):

We have established that at one month of age the corticomedullary junction is characterized by novel floret structures comprised of CD49+, PIGR+, and Cld3+ mTEC subsets. PIGR expression appears to be restricted to the florets at this stage and is therefore the best marker to use to identify and functionally characterize florets in future studies. The mTEC subsets are arranged in onion-like layers spanning from the cortical face of the floret inward towards the central medulla. The presence of CLD3+ mTEC (identified as medullary progenitors [58]) within the florets suggests that these florets could be sites of mTEC generation. Each floret has vascular input stemming from the central medulla. The large vessels in the central medulla are wrapped by CD49+ sTECs. What is intriguing is

that sTEC expression stops short of the vasculature that extends into the florets but is also expressed highly at the cortical facing surface of the floret. This result suggests that the florets serve as potential sites where cells can enter and exit the thymus at the CMJ. CD49+ sTEC are also associated closely with cortical capillaries, which further supports the idea that trafficking is directed towards the florets in the CMJ. In addition to vasculature inputs from the central medulla each floret has neurites entering from the cortex, which are presumably CHAT+, the function of which is unknown. Doublecortin+ cells previously identified as tuft cells exist in a layer interior to the florets at the CMJ, as individual scattered cells. These cells express high levels of IL-25 and are thought to maintain a niche for NKT cells and potentially Tregs [91,92]. While this is an intriguing prospect additional experiments are required to validate this finding.

NF+ mTEC are located interior to the DC+ tuft cell layer. NF has been identified as a FOXN1 direct target [26], and NF expression has been shown in mTEChi cells in a gene expression analysis at 1 month [93], confirming our identification of these NF+ cells as mTECs. It is unclear how these cells fit into the four postnatal mTEC subsets identified by scRNA-seq [56]. AIRE+ mTEC are confined to and present throughout the medulla, consistent with previous data [94]. K14 is expressed throughout the medulla but is low or undetectable in most or all PIGR+, DC+, CD49+, and NF+ mTECs. Interestingly in the early stages of thymic involution many of these aforementioned features are either lost of lack the organization that is present in the steady-state thymus. The florets have emerged as a striking feature in the steady-state thymus and the localization of these structures at the CMJ suggests that they may play an important role in trafficking of thymocytes and/or

as establishing stem cell niches making future functional characterizations of these geographical features vitally important to the field of thymus biology.

During the neonatal period and perinatal to adult transition (P0-P14):

At P0, NF+ clusters of mTECs are present near the CMJ, prior to any PIGR expression or other floret characteristics. The thymic vasculature at P0 has the characteristic 'broccoli-like' arrangement of large vessels in the deeper medulla, branching outward to the capillary bed in the cortex. The P0 thymus contains lymphatic vessels located in the central deep medulla, which have not previously been investigated in the thymus. The thymus is extensively innervated in the capsule cortex and medullary regions with NF+ fibers at P0. By P7, CD49+ sTEC are found throughout the cortical capillary bed, and small clusters of mTECs are beginning to form floret-like structures. Spatially these structures are associated with NF+ mTEC clusters (that were present at P0). Many of the NF negative mTEC in these nascent florets express combinations of PIGR, AIRE, CD49 and DC, with some cells that express individual markers. NF+ fibers are found throughout the capsule cortex and medulla and cortical fibers are detected projecting into the nascent florets at P7. By P14, the nascent floret structures are starting to resemble features of the steady-state florets, including PIGR+ and CD49+ mTEC, and excluding AIRE, with DC+ cells scattered in a layer internal to the medulla.

Further investigation is required to determine the functional importance the NF+ fibers may play in floret patterning, function, or a combination of both. The idea that the nervous system could be modulating specialized TEC geographical features and the mechanisms by which they may drive the function or developmental patterning of these features is an entirely novel hypothesis that warrants further experimentation.

Features that are dependent on Foxn1 function (from the Foxn1$^{Z/Z}$ mice):

The most noticeable difference in the *Foxn1*$^{Z/Z}$ mutants compared to their WT counterparts at P0 is the absence of NF+ mTEC at all stages. This finding is consistent with NF being a direct target of FOXN1 [26]. Innervation of the capsule cortex and medulla is also markedly reduced relative to wild-type in mutants. Another defining difference of the *Foxn1*$^{Z/Z}$ mutants is an irregularly patterned vasculature network, that features fewer large vessels in the central medulla., consistent with FOXN1's known role in vascular patterning in the thymus [45]. Not surprisingly since lymphatic vessels are located within the deep medulla and colocalized with large vasculature vessels the *Foxn1*$^{Z/Z}$ mutants seemingly lack deep medulla lymphatic networks. As the function of lymphatics in the thymus is unknown, the functional implications of this phenotype are unclear. Medullary organization as surveyed through the expression of K14 is also divergent from WT as it is not only expressed at higher levels but is also less uniform and patchier than WT. At P7 individual PIGR+, AIRE+, and DC+ cells are present, with few or no cells expressing multiple markers as seen in wild-type nascent florets at this stage. These cells are also not organized well into clusters, with PIGR+ cells scattered throughout the outer medulla and some in the central region. This result suggests not only a failure to form proper florets but also an early differentiation of the mTEC subsets. In terms of innervation there are few neurites observed projecting from the cortex into the CMJ region at P7 but the capsule region is still innervated. By P14, the *Foxn1*$^{Z/Z}$ mutant thymus is highly disorganized, with no identifiable florets or other clear organizational structures that are present in the wild-type at this stage or the 1-month stage. P14 *Foxn1*$^{Z/Z}$ mutants resemble 3-month wild-type thymi, consistent with the previously assessed expression of Foxn1 at P7 in the mutants

being reduced similar to 3-months levels in wild-type [80]. These data suggest that floret formation is dependent on NF+ mTEC pre-patterning in the perinatal period, which is controlled by FOXN1.

Future Directions

The new observations and conclusions listed above support and suggest a wealth of new hypotheses and directions for future work to investigate the functional organization of the thymus and how it changes over the lifespan, as well as the role of FOXN1 during this period, some of which are listed below:

Trafficking and Migration

The trafficking of cells in and out of the thymus is vital to a properly function immune system. We have shown that CD49+ sTEC are found in the deep medulla and the cortical capillary bed wrapping vasculature. This phenomenon is especially intriguing because Claudin 5, an established tight junction and blood brain barrier (BBB) marker is expressed in similar patterns in the deep medulla and cortical capillary bed in thymic vasculature. Together this suggests that sTECs may be working in concert with endothelial cells to regulate the recruiting and transferring of cells in and out of the thymus. Specifically, the florets could be the site of lymphocyte progenitors entering and mature naïve T cells exiting the thymus, and thus acting as ‘gatekeepers’ of T cell generation.

Neuromodulation of Thymus Development and Function

The NF+ mTEC populations and neurites from the cortex offer another intriguing route of investigation as they could connect and induce the patterning of the CMJ during the perinatal time period. This possibility could provide a testable hypothesis for the role

of thymic innervation, that is not currently understood and could offer great insight into neuromodulation on the immune system.

Generation of Specialized Niches

The florets could be sites in which specific functional cellular neighborhoods, or niches, form. The presence of CLD3 in the florets at the CMJ suggests that these florets are the site of mTEC homeostasis, as these established mTEC progenitors are localized within these structures. The fact that CD49 is a known cell adhesion molecule that is involved in maintaining stem cell niche microenvironments in other organs and in human makes this an even more tantalizing prospect for further investigation. While not inside the floret, the presence of DC+ tuft cells beneath the florets could possibly define another niche that is responsible for NK T cell development, due to their production of IL25.

Disorganization of Florets Represent Early Signs of Involution

The loss of the floret and medullary layer structures could be critical hallmarks of early changes in medullary function during involution. Functionally characterizing the florets and their disorganization in conjunction with established features of involution such as decreased cellularity and increased adipogenesis would establish a more detailed timeline of involution. The loss of the floret and medullary layer structures could be critical hallmarks of early changes in medullary function during involution. Monitoring these multicellular structures could be important to evaluate strategies to maintain optimal thymus function, regenerate thymus function after aging or damage, or create de novo thymus function from organoids *in vitro* or *in vivo*.

REFERENCES

1. Petrie HT, Zuniga-Pflucker JC (2007) Zoned out: functional mapping of stromal signaling microenvironments in the thymus. Annu Rev Immunol 25: 649-679.

2. Anderson G, Takahama Y (2012) Thymic epithelial cells: working class heroes for T cell development and repertoire selection. Trends Immunol 33: 256-263.

3. Shah DK, Zuniga-Pflucker JC (2014) An overview of the intrathymic intricacies of T cell development. J Immunol 192: 4017-4023.

4. Halkias J, Melichar HJ, Taylor KT, Robey EA (2014) Tracking migration during human T cell development. Cell Mol Life Sci 71: 3101-3117.

5. Garfin PM, Min D, Bryson JL, Serwold T, Edris B, Blackburn CC, Richie ER, Weinberg KI, Manley NR, Sage J, Viatour P (2013) Inactivation of the RB family prevents thymus involution and promotes thymic function by direct control of Foxn1 expression. The Journal of experimental medicine 210: 1087-1097.

6. Robles AI, Larcher F, Whalin RB, Murillas R, Richie E, Gimenez-Conti IB, Jorcano JL, Conti CJ (1996) Expression of cyclin D1 in epithelial tissues of transgenic mice results in epidermal hyperproliferation and severe thymic hyperplasia. Proc Natl Acad Sci U S A 93: 7634-7638.

7. Takahama Y (2006) Journey through the thymus: stromal guides for T-cell development and selection. Nat Rev Immunol 6: 127-135.

8. Weinshenker BG, Penman M, Bass B, Ebers GC, Rice GP (1992) A double-blind, randomized, crossover trial of pemoline in fatigue associated with multiple sclerosis. Neurology 42: 1468-1471.

9. Lind EF, Prockop SE, Porritt HE, Petrie HT (2001) Mapping precursor movement through the postnatal thymus reveals specific microenvironments supporting defined stages of early lymphoid development. J Exp Med 194: 127-134.

10. Haynes L, Swain SL (2006) Why aging T cells fail: implications for vaccination. Immunity 24: 663-666.

11. Taub DD, Longo DL (2005) Insights into thymic aging and regeneration. Immunol Rev 205: 72-93.

12. Griffith AV, Fallahi M, Venables T, Petrie HT (2012) Persistent degenerative changes in thymic organ function revealed by an inducible model of organ regrowth. Aging Cell 11: 169-177.

13. Manley NR, Condie BG (2010) Transcriptional regulation of thymus organogenesis and thymic epithelial cell differentiation. Prog Mol Biol Transl Sci 92: 103-120.

14. Nehls M, Pfeifer D, Schorpp M, Hedrich H, Boehm T (1994) New member of the winged-helix protein family disrupted in mouse and rat nude mutations. Nature 372: 103-107.

15. Gordon J, Bennett AR, Blackburn CC, Manley NR (2001) Gcm2 and Foxn1 mark early parathyroid- and thymus-specific domains in the developing third pharyngeal pouch. Mech Dev 103: 141-143.

16. Cheng L, Guo J, Sun L, Fu J, Barnes PF, Metzger D, Chambon P, Oshima RG, Amagai T, Su DM (2010) Postnatal tissue-specific disruption of transcription factor FoxN1 triggers acute thymic atrophy. J Biol Chem 285: 5836-5847.

17. Ortman CL, Dittmar KA, Witte PL, Le PT (2002) Molecular characterization of the mouse involuted thymus: aberrations in expression of transcription regulators in thymocyte and epithelial compartments. Int Immunol 14: 813-822.

18. Chen ZF, Mao L, Liu LM, Liu YC, Peng Y, Hong X, Wang HH, Liu HG, Liang H Potential new inorganic antitumour agents from combining the anticancer traditional Chinese medicine (TCM) matrine with Ga(III), Au(III), Sn(IV) ions, and DNA binding studies. J Inorg Biochem 105: 171-180.

19. Manley NR, Richie ER, Blackburn CC, Condie BG, Sage J (2012) Structure and function of the thymic microenvironment. Front Biosci 17: 2461-2477.

20. Zook EC, Krishack PA, Zhang S, Zeleznik-Le NJ, Firulli AB, Witte PL, Le PT (2011) Overexpression of Foxn1 attenuates age-associated thymic involution and prevents the expansion of peripheral CD4 memory T cells. Blood 118: 5723-5731.

21. Bredenkamp N, Ulyanchenko S, O'Neill KE, Manley NR, Vaidya HJ, Blackburn CC (2014) An organized and functional thymus generated from FOXN1-reprogrammed fibroblasts. Nat Cell Biol 16: 902-908.

22. Blackburn CC, Augustine CL, Li R, Harvey RP, Malin MA, Boyd RL, Miller JF, Morahan G (1996) The nu gene acts cell-autonomously and is required for differentiation of thymic epithelial progenitors. Proc Natl Acad Sci U S A 93: 5742-5746.

23. Nowell CS, Bredenkamp N, Tetelin S, Jin X, Tischner C, Vaidya H, Sheridan JM, Stenhouse FH, Heussen R, Smith AJ, Blackburn CC (2011) Foxn1 regulates lineage progression in cortical and medullary thymic epithelial cells but is dispensable for medullary sublineage divergence. PLoS Genet 7: e1002348.

24. Nehls M, Kyewski B, Messerle M, Waldschutz R, Schuddekopf K, Smith AJ, Boehm T (1996) Two genetically separable steps in the differentiation of thymic epithelium. Science 272: 886-889.

25. Su DM, Navarre S, Oh WJ, Condie BG, Manley NR (2003) A domain of Foxn1 required for crosstalk-dependent thymic epithelial cell differentiation. Nat Immunol 4: 1128-1135.

26. Zuklys S, Handel A, Zhanybekova S, Govani F, Keller M, Maio S, Mayer CE, Teh HY, Hafen K, Gallone G, Barthlott T, Ponting CP, Hollander GA (2016) Foxn1 regulates key target genes essential for T cell development in postnatal thymic epithelial cells. Nat Immunol 17: 1206-1215.

27. Weinberg RA (1995) The retinoblastoma protein and cell cycle control. Cell 81: 323-330.

28. Lim S, Kaldis P (2013) Cdks, cyclins and CKIs: roles beyond cell cycle regulation. Development 140: 3079-3093.

29. Sun A, Bagella L, Tutton S, Romano G, Giordano A (2007) From G0 to S phase: a view of the roles played by the retinoblastoma (Rb) family members in the Rb-E2F pathway. J Cell Biochem 102: 1400-1404.

30. Iaquinta PJ, Lees JA (2007) Life and death decisions by the E2F transcription factors. Curr Opin Cell Biol 19: 649-657.

31. Chinnam M, Goodrich DW (2011) RB1, development, and cancer. Curr Top Dev Biol 94: 129-169.

32. Stevens C, La Thangue NB (2003) E2F and cell cycle control: a double-edged sword. Arch Biochem Biophys 412: 157-169.

33. Mulhern DM, Jones EB (2005) Test of revised method of age estimation from the auricular surface of the ilium. Am J Phys Anthropol 126: 61-65.

34. Frolov MV, Dyson NJ (2004) Molecular mechanisms of E2F-dependent activation and pRB-mediated repression. J Cell Sci 117: 2173-2181.

35. Dimova DK, Dyson NJ (2005) The E2F transcriptional network: old acquaintances with new faces. Oncogene 24: 2810-2826.

36. Giroud C, Augsburger M, Menetrey A, Mangin P (2003) Determination of zaleplon and zolpidem by liquid chromatography-turbo-ionspray mass spectrometry: application to forensic cases. J Chromatogr B Analyt Technol Biomed Life Sci 789: 131-138.

37. Cobrinik D (2005) Pocket proteins and cell cycle control. Oncogene 24: 2796-2809.

38. Ferreira R, Magnaghi-Jaulin L, Robin P, Harel-Bellan A, Trouche D (1998) The three members of the pocket proteins family share the ability to repress E2F activity through recruitment of a histone deacetylase. Proc Natl Acad Sci U S A 95: 10493-10498.

39. Lechner MS, Schultz DC, Negorev D, Maul GG, Rauscher FJ, 3rd (2005) The mammalian heterochromatin protein 1 binds diverse nuclear proteins through a common motif that targets the chromoshadow domain. Biochem Biophys Res Commun 331: 929-937.

40. Azzarelli R, Hardwick LJ, Philpott A (2015) Emergence of neuronal diversity from patterning of telencephalic progenitors. Wiley Interdiscip Rev Dev Biol 4: 197-214.

41. Ali F, Hindley C, McDowell G, Deibler R, Jones A, Kirschner M, Guillemot F, Philpott A (2011) Cell cycle-regulated multi-site phosphorylation of Neurogenin 2 coordinates cell cycling with differentiation during neurogenesis. Development 138: 4267-4277.

42. Davidson G, Niehrs C (2010) Emerging links between CDK cell cycle regulators and Wnt signaling. Trends Cell Biol 20: 453-460.

43. Weinstein N, Ortiz-Gutierrez E, Munoz S, Rosenblueth DA, Alvarez-Buylla ER, Mendoza L (2015) A model of the regulatory network involved in the control of the cell cycle and cell differentiation in the Caenorhabditis elegans vulva. BMC Bioinformatics 16: 81.

44. Viatour P, Somervaille TC, Venkatasubrahmanyam S, Kogan S, McLaughlin ME, Weissman IL, Butte AJ, Passegue E, Sage J (2008) Hematopoietic stem cell quiescence is maintained by compound contributions of the retinoblastoma gene family. Cell Stem Cell 3: 416-428.

45. Bryson JL, Griffith AV, Hughes B, 3rd, Saito F, Takahama Y, Richie ER, Manley NR (2013) Cell-autonomous defects in thymic epithelial cells disrupt endothelial-perivascular cell interactions in the mouse thymus. PloS one 8: e65196.

46. Anderson G, Harman BC, Hare KJ, Jenkinson EJ (2000) Microenvironmental regulation of T cell development in the thymus. Semin Immunol 12: 457-464.

47. Yuan J, Nguyen CK, Liu X, Kanellopoulou C, Muljo SA (2012) Lin28b reprograms adult bone marrow hematopoietic progenitors to mediate fetal-like lymphopoiesis. Science 335: 1195-1200.

48. Cuddihy AR, Ge S, Zhu J, Jang J, Chidgey A, Thurston G, Boyd R, Crooks GM (2009) VEGF-mediated cross-talk within the neonatal murine thymus. Blood 113: 2723-2731.

49. Gordon J, Wilson VA, Blair NF, Sheridan J, Farley A, Wilson L, Manley NR, Blackburn CC (2004) Functional evidence for a single endodermal origin for the thymic epithelium. Nat Immunol 5: 546-553.

50. van Ewijk W, Shores EW, Singer A (1994) Crosstalk in the mouse thymus. Immunol Today 15: 214-217.

51. Venables T, Griffith AV, DeAraujo A, Petrie HT (2019) Dynamic changes in epithelial cell morphology control thymic organ size during atrophy and regeneration. Nat Commun 10: 4402.

52. Odaka C, Loranger A, Takizawa K, Ouellet M, Tremblay MJ, Murata S, Inoko A, Inagaki M, Marceau N (2013) Keratin 8 is required for the maintenance of architectural structure in thymus epithelium. PLoS One 8: e75101.

53. Jenkinson WE, Nakamura K, White AJ, Jenkinson EJ, Anderson G (2012) Normal T Cell Selection Occurs in CD205-Deficient Thymic Microenvironments. PLoS One 7: e53416.

54. Gray DH, Chidgey AP, Boyd RL (2002) Analysis of thymic stromal cell populations using flow cytometry. J Immunol Methods 260: 15-28.

55. Ripen AM, Nitta T, Murata S, Tanaka K, Takahama Y (2011) Ontogeny of thymic cortical epithelial cells expressing the thymoproteasome subunit beta5t. Eur J Immunol 41: 1278-1287.

56. Bornstein C, Nevo S, Giladi A, Kadouri N, Pouzolles M, Gerbe F, David E, Machado A, Chuprin A, Toth B, Goldberg O, Itzkovitz S, Taylor N, Jay P, Zimmermann VS, Abramson J, Amit I (2018) Single-cell mapping of the thymic stroma identifies IL-25-producing tuft epithelial cells. Nature 559: 622-626.

57. Kadouri N, Nevo S, Goldfarb Y, Abramson J (2020) Thymic epithelial cell heterogeneity: TEC by TEC. Nat Rev Immunol 20: 239-253.

58. Hamazaki Y, Fujita H, Kobayashi T, Choi Y, Scott HS, Matsumoto M, Minato N (2007) Medullary thymic epithelial cells expressing Aire represent a unique lineage derived from cells expressing claudin. Nat Immunol 8: 304-311.

59. Mori K, Itoi M, Tsukamoto N, Amagai T (2010) Foxn1 is essential for vascularization of the murine thymus anlage. Cell Immunol 260: 66-69.

60. Bryson JL, Coles MC, Manley NR (2011) A method for labeling vasculature in embryonic mice. J Vis Exp.

61. Schwab SR, Cyster JG (2007) Finding a way out: lymphocyte egress from lymphoid organs. Nature immunology 8: 1295-1301.

62. Cyster JG, Schwab SR (2012) Sphingosine-1-phosphate and lymphocyte egress from lymphoid organs. Annu Rev Immunol 30: 69-94.

63. Kurd N, Robey EA (2016) T-cell selection in the thymus: a spatial and temporal perspective. Immunol Rev 271: 114-126.

64. Carmeliet P, Tessier-Lavigne M (2005) Common mechanisms of nerve and blood vessel wiring. Nature 436: 193-200.

65. Bockman DE, Kirby ML (1984) Dependence of thymus development on derivatives of the neural crest. Science 223: 498-500.

66. Kuratani S, Bockman DE (1990) Impaired development of the thymic primordium after neural crest ablation. Anat Rec 228: 185-190.

67. Mignini F, Sabbatini M, Mattioli L, Cosenza M, Artico M, Cavallotti C (2014) Neuro-immune modulation of the thymus microenvironment (review). Int J Mol Med 33: 1392-1400.

68. Tollefson L, Bulloch K (1990) Dual-label retrograde transport: CNS innervation of the mouse thymus distinct from other mediastinum viscera. J Neurosci Res 25: 20-28.

69. Bulloch K, Cullen MR, Schwartz RH, Longo DL (1987) Development of innervation within syngeneic thymus tissue transplanted under the kidney capsule of the nude mouse: a light and ultrastructural microscope study. J Neurosci Res 18: 16-27.

70. Hu D, Nicholls PK, Yin C, Kelman K, Yuan Q, Greene WK, Shi Z, Ma B (2018) Immunofluorescent Localization of Non-myelinating Schwann Cells and Their Interactions With Immune Cells in Mouse Thymus. J Histochem Cytochem 66: 775-785.

71. Erturk A, Becker K, Jahrling N, Mauch CP, Hojer CD, Egen JG, Hellal F, Bradke F, Sheng M, Dodt HU (2012) Three-dimensional imaging of solvent-cleared organs using 3DISCO. Nat Protoc 7: 1983-1995.

72. Chung K, Deisseroth K (2013) CLARITY for mapping the nervous system. Nat Methods 10: 508-513.

73. Yang B, Treweek JB, Kulkarni RP, Deverman BE, Chen CK, Lubeck E, Shah S, Cai L, Gradinaru V (2014) Single-cell phenotyping within transparent intact tissue through whole-body clearing. Cell 158: 945-958.

74. Tainaka K, Kubota SI, Suyama TQ, Susaki EA, Perrin D, Ukai-Tadenuma M, Ukai H, Ueda HR (2014) Whole-body imaging with single-cell resolution by tissue decolorization. Cell 159: 911-924.

75. Jing D, Zhang S, Luo W, Gao X, Men Y, Ma C, Liu X, Yi Y, Bugde A, Zhou BO, Zhao Z, Yuan Q, Feng JQ, Gao L, Ge WP, Zhao H (2018) Tissue clearing of both hard and soft tissue organs with the PEGASOS method. Cell Res 28: 803-818.

76. Perry JS, Lio CW, Kau AL, Nutsch K, Yang Z, Gordon JI, Murphy KM, Hsieh CS (2014) Distinct contributions of Aire and antigen-presenting-cell subsets to the generation of self-tolerance in the thymus. Immunity 41: 414-426.

77. Brekelmans P, van Ewijk W (1990) Phenotypic characterisation of murine thymic microenvironments. seminars in Immunology 2: 13 - 24.

78. Anderson M, Anderson SK, Farr AG (2000) Thymic vasculature: organizer of the medullary epithelial compartment? Int Immunol 12: 1105-1110.

79. Chinn IK, Blackburn CC, Manley NR, Sempowski GD (2012) Changes in primary lymphoid organs with aging. Seminars in immunology 24: 309-320.

80. Sun L, Guo J, Brown R, Amagai T, Zhao Y, Su DM (2010) Declining expression of a single epithelial cell-autonomous gene accelerates age-related thymic involution. Aging Cell 9: 347-357.

81. Gardner JM, Fletcher AL, Anderson MS, Turley SJ (2009) AIRE in the thymus and beyond. Curr Opin Immunol 21: 582-589.

82. Klug DB, Carter C, Crouch E, Roop D, Conti CJ, Richie ER (1998) Interdependence of cortical thymic epithelial cell differentiation and T-lineage commitment. Proc Natl Acad Sci U S A 95: 11822-11827.

83. Sakata M, Ohigashi I, Takahama Y (2018) Cellularity of Thymic Epithelial Cells in the Postnatal Mouse. J Immunol 200: 1382-1388.

84. Nance DM, Sanders VM (2007) Autonomic innervation and regulation of the immune system (1987-2007). Brain Behav Immun 21: 736-745.

85. Al-Shalan HAM, Hu D, Nicholls PK, Greene WK, Ma B (2019) Immunofluorescent characterization of innervation and nerve-immune cell neighborhood in mouse thymus. Cell Tissue Res 378: 239-254.

86. Elenkov IJ, Wilder RL, Chrousos GP, Vizi ES (2000) The sympathetic nerve--an integrative interface between two supersystems: the brain and the immune system. Pharmacol Rev 52: 595-638.

87. Madden KS, Bellinger DL, Felten SY, Snyder E, Maida ME, Felten DL (1997) Alterations in sympathetic innervation of thymus and spleen in aged mice. Mech Ageing Dev 94: 165-175.

88. Bulloch K, Moore RY (1981) Innervation of the thymus gland by brain stem and spinal cord in mouse and rat. Am J Anat 162: 157-166.

89. Chen L, Xiao S, Manley NR (2009) Foxn1 is required to maintain the postnatal thymic microenvironment in a dosage-sensitive manner. Blood 113: 567-574.

90. Gonzalez-Garcia S, Garcia-Peydro M, Martin-Gayo E, Ballestar E, Esteller M, Bornstein R, de la Pompa JL, Ferrando AA, Toribio ML (2009) CSL-MAML-dependent Notch1 signaling controls T lineage-specific IL-7R{alpha} gene expression in early human thymopoiesis and leukemia. J Exp Med 206: 779-791.

91. Wang H, Breed ER, Lee YJ, Qian LJ, Jameson SC, Hogquist KA (2019) Myeloid cells activate iNKT cells to produce IL-4 in the thymic medulla. Proc Natl Acad Sci U S A 116: 22262-22268.

92. Wegehaupt O, Wustrau K, Lehmberg K, Ehl S (2020) Cell Versus Cytokine - Directed Therapies for Hemophagocytic Lymphohistiocytosis (HLH) in Inborn Errors of Immunity. Front Immunol 11: 808.

93. Ki S, Park D, Selden HJ, Seita J, Chung H, Kim J, Iyer VR, Ehrlich LI (2014) Global transcriptional profiling reveals distinct functions of thymic stromal subsets and age-related changes during thymic involution. Cell Rep 9: 402-415.

94. Zuklys S, Balciunaite G, Agarwal A, Fasler-Kan E, Palmer E, Hollander GA (2000) Normal thymic architecture and negative selection are associated with Aire expression, the gene defective in the autoimmune-polyendocrinopathy-candidiasis-ectodermal dystrophy (APECED). J Immunol 165: 1976-1983.